27
3-4-76
NTIS

ORNL/TM-5210

Cryogenic Power Transmission Technology—Cryogenic Dielectrics

Quarterly Report
April 1–June 30, 1975

MASTER

OAK RIDGE NATIONAL LABORATORY
OPERATED BY UNION CARBIDE CORPORATION FOR THE ENERGY RESEARCH AND DEVELOPMENT ADMINISTRATION

DISTRIBUTION OF THIS DOCUMENT IS UNLIMITED

DISCLAIMER

This report was prepared as an account of work sponsored by an agency of the United States Government. Neither the United States Government nor any agency Thereof, nor any of their employees, makes any warranty, express or implied, or assumes any legal liability or responsibility for the accuracy, completeness, or usefulness of any information, apparatus, product, or process disclosed, or represents that its use would not infringe privately owned rights. Reference herein to any specific commercial product, process, or service by trade name, trademark, manufacturer, or otherwise does not necessarily constitute or imply its endorsement, recommendation, or favoring by the United States Government or any agency thereof. The views and opinions of authors expressed herein do not necessarily state or reflect those of the United States Government or any agency thereof.

DISCLAIMER

Portions of this document may be illegible in electronic image products. Images are produced from the best available original document.

Printed in the United States of America. Available from
National Technical Information Service
U.S. Department of Commerce
5285 Port Royal Road, Springfield, Virginia 22161
Price: Printed Copy $6.00 ; Microfiche $2.25

This report was prepared as an account of work sponsored by the United States Government. Neither the United States nor the Energy Research and Development Administration, nor any of their employees, nor any of their contractors, subcontractors, or their employees, makes any warranty, express or implied, or assumes any legal liability or responsibility for the accuracy, completeness or usefulness of any information, apparatus, product or process disclosed, or represents that its use would not infringe privately owned rights.

ORNL/TM-5210

Contract No. W-7405-eng-26

Activity No. JP 02 03 00 0

CRYOGENIC POWER TRANSMISSION TECHNOLOGY — CRYOGENIC DIELECTRICS

Quarterly Report

April 1 - June 30, 1975

Cryoelectrics Section
Engineering Sciences Group
Thermonuclear Division

FEBRUARY 1976

NOTICE
This report was prepared as an account of work sponsored by the United States Government. Neither the United States nor the United States Energy Research and Development Administration, nor any of their employees, nor any of their contractors, subcontractors, or their employees, makes any warranty, express or implied, or assumes any legal liability or responsibility for the accuracy, completeness or usefulness of any information, apparatus, product or process disclosed, or represents that its use would not infringe privately owned rights.

OAK RIDGE NATIONAL LABORATORY
Oak Ridge, Tennessee 37830
operated by
UNION CARBIDE CORPORATION
for the
ENERGY RESEARCH AND DEVELOPMENT ADMINISTRATION

DISTRIBUTION OF THIS DOCUMENT IS UNLIMITED

THIS PAGE

WAS INTENTIONALLY

LEFT BLANK

TABLE OF CONTENTS

ABSTRACT. v

I. CRYOGENIC DIELECTRICS 1

APPENDIX A. 22

REFERENCES. 23

FIGURE CAPTIONS 24

II. AC LOSSES IN SUPERCONDUCTORS. 31

APPENDIX A. 51

APPENDIX B. 53

REFERENCES. 56

FIGURE CAPTIONS 57

III. DISPERSION HARDENING OF ALUMINUM. 69

REFERENCES. 78

FIGURE CAPTIONS 79

THIS PAGE

WAS INTENTIONALLY

LEFT BLANK

Abstract

During this reporting period, April 1 to June 30, 1975, ac dielectric breakdown and partial discharge measurements were carried out on several new polyolefin films immersed in liquid helium at atmospheric pressure. The average breakdown strengths ranged from 135 to 220 MV/m, and were close to the breakdown strengths for the other materials already tested. Analysis of the partial discharge inception voltages for all of the materials tested so far shows that the major determinant of partial discharge inception is the breakdown voltage of the helium layer in series with the film.

In other experiments on Valeron polyethylene with both film and electrodes completely encapsulated by epoxy, breakdown occurred with no observable partial discharge. The partial discharge sensitivity was the same as used for the unencapsulated film experiments. The breakdown strength with encapsulation was slightly higher than without. The temperature was varied from 4.2 K to 300 K, but no influence on the breakdown strength was observed.

Breakdown tests with ac voltage were carried out on liquid helium between ASTM electrodes. The peak breakdown voltages measured on the first run were somewhat lower than the previously measured dc voltages. After repolishing the electrodes, another run in which both dc and ac breakdown voltages were taken showed good agreement. However, the voltages were now about 30% higher than those of the first run, and were close to the ASTM standard for C-10 oil. It is suspected that contamination in the helium is responsible for the variable results.

Progress is reported in the construction of the High Voltage Cryostat. A lifting mechanism for the large dewar tank is being fabricated, and the vacuum system is complete. Both of the small cryostats IV1 and IV2 were operated successfully during the quarter, although IV2 eventually failed during ac operation above 50 kV rms. IV3, the 33 cm diameter cryostat, will soon be ready for leak checking.

The fabrication and oil impregnation were completed on a new Kraft paper interwinding insulation cylinder for transformer B of the Hipotronics 700 kV ac test set, and final reassembly will begin soon.

As of the end of this reporting period, the program on ac losses in superconductors was terminated by decision of ERDA-DEES. The final report of this project summarizes measurements of the ac losses in Nb_3Sn prepared by several different methods. An electronic method was used in which the losses were detected by a lock-in amplifier connected to appropriate pickup coils wound around the sample. A correction was applied for eddy current losses in the pickup coils. The loss per unit area per cycle was found to be linearly dependent on applied field frequency, with a considerable hysteretic component remaining at zero frequency. The hysteretic component was about two orders of magnitude lower for Nb_3Sn prepared by a solid state diffusion method than for material formed by tin-plating a niobium sample, with similar reaction heat treatments in both cases. Higher hysteretic losses were associated with greater surface roughness of the sample. In contrast, the frequency-dependent loss contribution did not appear to be strongly influenced by surface roughness.

Measurements on Mo-25 Re, a material known to have overwhelmingly hysteretic losses, showed no obvious frequency dependence at any field amplitude over the frequency range investigated (40-100 Hz). Hence the frequency-dependent losses observed with Nb_3Sn are not a systematic effect originating in the apparatus.

In the aluminum dispersion hardening studies, measurements of residual resistivity ratio (RRR) vs aging time at various temperatures have been carried out for alloys with several different gold concentrations. The RRR increased with aging time, and the ultimate total increase was greater the higher the aging temperature. An alloy with 0.12 wt % gold aged 1000 hr at 300°C showed the largest RRR increase observed, a factor of 23.

Preliminary tensile tests have been carried out on the 0.12 wt % alloy. However, due to slippage of tensile tester grips, the data is not yet reliable.

Microhardness measurements on a 0.26 wt % alloy showed a prominent hardness maximum after 10 hrs aging at 187°C. More extensive measurements were hampered by the lack of suitable flat, parallel-sided specimens which are now being fabricated.

Several commercial fiber-reinforced aluminum composites were procured for RRR tests. The values observed were between 2 and 115 and thus far below the high RRR standards required for a cable conductor substrate. New fiber-reinforced composites are being fabricated in-house with the same high RRR aluminum as used in the dispersion hardening experiments.

I. CRYOGENIC DIELECTRICS

A. Activity During Quarter

1. Experimental Equipment

a) High Voltage Cryostats:

Fig. 1 is a photograph showing the present status of the High Voltage Cryostat. The vacuum system has been completed, and the inner tank and room temperature bushing have been evacuated to better than 10^{-5} torr with the diffusion pump and leak tested. A few electrical circuits for remote control of the large gate valves and for vacuum gauge instrumentation remain to be installed. A lifting mechanism for the dewar incorporating four chain-driven ball screw jacks has been designed and is under fabrication. The parts have been received for the 0.9 m diameter flat fiberglass head for closure of the bottom of the vacuum bushing, and this head is being assembled. We have placed inquiries with ITE and with Westinghouse regarding the purchase of a large conical insulator for higher pressures, and are waiting for replies.

b) Intermediate Voltage Cryostats:

As stated in the previous quarterly report, the helium dewar for IV2 was accidentally cracked during installation of the cryostat. A new dewar was ordered, and in the meantime IV2 was operated in the dewar for IV1. This did not greatly impede the experimental program, because experiments could be carried out in one cryostat while the electrodes or samples were being changed in the other. A pair of ASTM electrodes were mounted in IV2, and the bushing was successfully conditioned to 52 kV with ac voltage. The results of the ASTM ac experiments are reported in Section B.2. No unusual dissipation was found with ac

voltage. It appears that the source of the high dissipation observed earlier in IV1 was a very slow helium leak into the bushing vacuum. In the last of the ac experiments at a gap of 11 mm, the voltage was raised to 51 kV rms, and an arc inside the bushing produced a track on the G-10 disc. Evidently the safe voltage limits for IV1 and IV2 are about 100 kV dc and 45 kV rms ac. A new insulating disc made of Mycalex, a track-resistant material, was installed on IV2 but the epoxy seal between the disc and brass flange holding it leaked when the bushing was cooled. Although the expansion coefficient of Mycalex is close to that of brass at room temperature, it may be that excessive mismatch occurs at cryogenic temperatures. If attempts to repair the seal are not successful, another disc of G-10 fiberglass will be installed.

IV1 operated with no failures throughout the quarter, and was principally used for the breakdown tests on solid polymer films.

Assembly of IV3, the 33 cm diameter cryostat, has continued. Due to an engineering error in the shop drawings, the high voltage tube for the vacuum bushing was 2.5 cm too short. This tube has been lengthened, and the bushing should be ready for final leak checking early in the next quarter. All of the parts necessary for mounting electrodes or solid film samples are ready, and initial tests will begin as soon as the leak checks are complete.

c) Power Supplies:

The fabrication of a special cylinder of Kraft paper insulation for the repair of transformer B of the 700 kV ac Hipotronics test set was completed during this quarter. The insulating cylinder was built as described in the last quarterly report (see Appendix B, part II). The

vacuum and heating treatments were almost as described except that a vacuum of 0.3 torr was used and the time at vacuum was lengthened and interspersed with several flushes of dry nitrogen gas. The transformer oil used for impregnation contained 25 ppm of moisture before drying. After heat treatment at 40°C under a vacuum of 0.3 torr for 16 hours, the moisture content dropped to 10 ppm. The impregnation of the paper was carried out over a 16-hour period at 40°C under a vacuum of 0.35 to 0.4 torr. The newly impregnated paper cylinder will be assembled in the transformer during the next quarter.

The 250 kV, 600J impulse generator mentioned in the previous report is being built by the Universal Voltronics Corporation and is nearly ready for acceptance tests. A member of the group will visit the factory early in the next quarter to participate in these tests.

d) Instrumentation:

In order to measure peak impulse voltages accurately, a memory impulse voltmeter has been ordered from Ross Engineering Corporation. Delivery has been promised in November 1975. Other instrumentation orders include a PAR 122 lock-in amplifier, a high-speed oscilloscope camera for impulse studies, a helium flowmeter for boiloff rate measurements, and a true rms-to-dc converter.

2. Collaboration with Other Laboratories

On April 22, Blevins of ERDA-ORO, Long, Kernohan, Menon and Schwenterly attended a program review of the BNL SPTL Project. Although no formal discussions were held between ORNL and BNL personnel, it was suggested by E. Forsythe that the ORNL program also consider breakdown of solid dielectrics under fields with substantial components parallel

as well as perpendicular to the film surface. This information would be useful in the design of stress cones. Shortly after this meeting, several new polymer film samples were received from A. Muller of BNL. These included extra sheets of some of the materials tested in the last quarter, plus samples of four Cryovac polyolefin films. The results of tests on these materials are given in Section B.1. Several efforts were made to improve the experimental technique and arrive at values closer to the intrinsic dielectric strength of the film, and these are also discussed.

On the day following the BNL review, a visit was made to the Linde SPTL project at Tarrytown, New York. R. Meyerhoff and D. Bosack discussed their latest dielectric test results with liquid helium in the first subscale cable test sections, and gave us a preliminary written report. They expressed some concern that the observed impulse and ac flashover values were considerably lower than the previous results[1] obtained in liquid nitrogen with single spacers between sphere electrodes or with three spacers between coaxial electrodes.

Telephone contact was maintained with the LASL SPTL Project during the quarter. M. Maley informed us of their interest in a frozen oil impregnated paper dielectric from a suggestion by their consultant, E. Eich. However, so far no firm proposals for dielectrics research have been received from LASL. Near the end of the quarter, the LASL project hired P. Chowdhuri to manage the dielectric aspects of the program, and Chowdhuri is scheduled to visit us on July 29 to familiarize himself with our program and discuss possible areas for collaboration. The

possibility of a visit to LASL by our consultant G. L. Sommerman is also under discussion.

H. M. Long attended a progress review of the work on liquid helium fluid flow and heat transfer at NBS-Boulder in May. Hopefully some of the instrumentation for pressure, temperature, and flow measurement under development there will be of use in our programs.

A member of the group will attend the yearly progress review of the dielectric loss work at NBS-Gaithersburg on July 15. A sample of G-10 fiberglass-reinforced epoxy will be submitted for loss measurements in their new helium cryostat.

Requests for data on liquid helium breakdown were received from M. Rabinowitz of EPRI and E. Kessler of the National Accelerator Laboratory. We provided summaries of our own data as well as copies of other applicable papers from the literature.

On June 30, Long and Schwenterly attended a meeting at the ERDA-DEES offices to discuss further U.S.-Soviet cooperative efforts in SPTL research. The members of the team which visited the USSR at the end of March reported on their impressions of the trip and agreed to write up a summary of possible further benefits of the collaboration.

3. Other Activity

The prospective collaborations with LASL will make expansion of the group necessary if results are to be obtained within a reasonable amount of time. A job description for a second technician has been filed with the Laboratory Employment Department. We are also interviewing

candidates for another professional staff position. Dr. P. R. Emtage of Westinghouse Research Laboratories was interviewed on April 17-18, and Dr. T. S. Sudarshan of the National Research Council, Ottawa, Canada, visited on July 9-10.

S. W. Schwenterly attended a course on the Union Carbide Management System in eight full-day sessions, during the months of April, May and June.

Mr. P. O'Connor, an Oak Ridge Associated Universities summer student, is investigating the electric fields produced by two toroids at ground and high voltage, surrounding a dielectric rod. This geometry is being considered for surface flashover experiments in liquid helium. Mr. O'Connor is using the computer program by Dr. W. F. Westendorp which was described in our report for the first quarter of FY 1975 (ORNL-TM-4824). The results will be given in the next quarterly report.

An abstract of a paper on breakdown in polymer films was submitted for presentation at the 1975 NAS Conference on Electrical Insulation and Dielectric Phenomena, which will be held at NBS-Gaithersburg. This abstract appears in Appendix A.

B. Experimental Work

1. Polymer Film Tests

Two of the polymer film samples tested in the previous quarter (125-μm Nylon-11 and Hercules polypropylene) could not be broken down because heavy glow discharge around the epoxy-encapsulated high voltage electrode led to surface flashover before the breakdown voltage was reached.

No punctures were found either with the pinhole detector or by visual microscopy. Fig. 2 shows a view of one breakdown site on the 125-μm Nylon-11 sample, at a magnification of 100X. The bare tip of the circular electrode contacted the film in the central circular area, which shows only a few scratches and minor imperfections. Flashover tracks radiate out from the edge of the circle where the epoxy met the spherical electrode. The absence of punctures was verified by metallizing the sample and examining it for pinholes with back lighting.

Two schemes were tried to improve this situation. First a 125-μm Nylon-11 sample 12 cm in diameter was mounted with the high voltage electrode in the center to maximize the flashover distance. Even then, flashover occurred at between 16 and 17 kV, with no evidence of breakdown. Next, two 100-μm Valeron samples were completely encapsulated in epoxy, with six and eight sets of spherical electrodes respectively. Hence no helium could enter the region of high field gradient. Fig. 3a and Fig. 3b show an external view and an x-ray of Sample 2. With the first sample, all breakdown tests were made at helium temperature, while with the second, tests were carried out at room temperature and liquid nitrogen temperature as well. Table I summarizes the results.

Table I
Breakdown Tests with Encapsulated, 100-μm Van Leer Valeron HDPE

Sample	(K) T	(kV) V_b	(kV) V_{min}	(MV/m) E_b	(MV/m) E_{min}	No. Tests
1	4.2	15.6	12.5	158	127	6
2	301	18.5	18.4	187	186	2
	77	17.3	14.6	179	148	3
	4.2	14.5	10.2	147	103	3

In all cases, breakdown occurred with no audible or visible partial discharge (PD). Likewise, no evidence of PD was seen on the oscilloscope trace of the divider output. After testing, the epoxy blocks were split open and the breakdown sites were examined, as shown in Fig. 3a. Clean punctures were found between most of the spheres. For Sample 2, small bubbles in the epoxy were found at all of the sites (indicated by arrows in Fig. 3a) which gave minimum breakdown voltages. At the sites where the epoxy properly encapsulated the electrodes, the film withstood 18.4 kV to 18.6 kV (the highest voltage available with the transformer) for between 5 and 30 seconds before breaking down at all temperatures. Hence, the short-term intrinsic strength of a single 100-μm layer of Valeron polyethylene is about 185 MV/m and is relatively temperature independent. The values for Sample 1 were somewhat lower than for Sample 2, even though no bubbles were found in the epoxy. This might be due to indentation of the film by the electrodes, as discussed below. In any case, the breakdown voltages with both samples were higher than those measured with the earlier unencapsulated film method (see Fig. 4).

This encapsulated film test method is under further development to improve the casting techniques and eliminate bubbles or intrusion of the epoxy between the electrodes and film. Care must be taken not to force the electrodes together too strongly during casting to prevent them from indenting the film. With a 100-μm Valeron sample it was found that static forces larger than about 3 N on the 9.5 mm diameter electrodes would produce a permanent visible indentation. Measurements with a sensitive dial micrometer showed that dropping one of the 3.7 gm spheres onto the film from a height of 2.5 cm produced an indentation about 8 μm deep. Hence care is also necessary in assembling the electrodes into the mold to prevent damage to the film.

During the quarter a new set of plastic film samples was received from BNL. This included additional sheets of the materials tested last quarter plus samples of four new Cryovac polyolefin films in various thicknesses. The latter were immediately tested with a movable, epoxy-encapsulated sphere and a plane electrode in liquid helium boiling slowly at 1 atm, using the same techniques outlined in the previous quarterly report. Six breakdowns were taken with each polyolefin sample. The results are shown in Table II and in Fig. 4, which also gives the results for the materials tested previously for comparison. Breakdown and partial discharge (PD) onset voltages are read on the left hand scale, and breakdown electric fields on the right hand scale. The following points were noted for the polyolefin data:

TABLE II: Breakdown Tests with Cryovac Polyolefins

MATERIAL	(μm) t_n	(μm) t_a	(kV) PDIV Min	(kV) PDIV Av	(kV) PDIV %σ	(kV) PDEV Min	(kV) PDEV Av	(kV) PDEV %σ	(kV) V_{br} Min	(kV) V_{br} Av	(kV) V_{br} %σ	(MV/m) E_{br} Min	(MV/m) E_{br} Av	(MV/m) E_{pd}
Cryovac D-330 DW[1]	38	38	3.1	3.3	4.2	2.6	2.7		7.5	8.0	5.6	197	211	82
Cryovac D-330 SW	38	38	2.9	3.0	3.9	2.4	2.4	0.0	7.6	8.4	16.5	200	220	76
Cryovac D-330 SW[2]	38	38	3.0	3.2	3.9	2.4	2.5	3.2	4.6	6.4	19.2	121	168	79
Cryovac BB-Dykes-Silica	51	51	3.0	3.4	10.6	2.6	2.7	6.0	8.5	10.0	8.2	167	197	59
Cryovac BB-Dykes-Silica DW[3]	102	~111	5.3	5.6	4.7	4.4	4.8	6.9	13.8	15.0	11.5	124	135	48

COMMENTS:

1) Flashovers, between breakdown punctures. Scuffed surface.

2) Small projection on HV electrode - V_{br} rose w/succeeding tests. Note that PD voltages are unaffected.

3) Variation of thickness from 102μ to 142μ. 4 breakdowns only.

4) E_{pd} is the minimum partial discharge inception field strength.

a. The average breakdown strengths for single layers range from 135 MV/m to 220 MV/m. Even the minimum breakdown strengths are several times the BNL design figure of 10 MV/m. In general, the breakdown strengths fall with increasing film thickness. The polyolefins are considerably better than Nylon-11 for the 38-μm samples. However, the 51-μm sample has a breakdown strength significantly lower than that of a similar thickness of Nylon-11. The 111-μm sample showed a breakdown strength in between Van Leer Valeron polyethylene and Rowland polysulfone.

b. The PD inception voltages for the polyolefins were again about one-third to one-half the breakdown voltages. The extinction voltages were all about 20% lower than the inception voltages. The minimum inception field strengths range from about 50 to 80 MV/m. Like the breakdown strengths, they fall off as the film thickness increases. It can be seen that at a given thickness, the material with the highest breakdown voltage does not necessarily have the highest PD inception voltage. Furthermore, in the second D-330-SW sample, a small projection which penetrated the polymer slightly was inadvertently left at the center of the high voltage electrode. This lowered the breakdown stress considerably, but left the PD inception and extinction voltages unchanged. An analogous situation in a real cable might be a small metal particle between the dielectric and conductor. This indicates that in the cable such particles against the conductor might not show up in a PD inception voltage test. Normal operation of the cable would not be

impaired, since it must operate below the inception voltage, but the resistance to transient overvoltages might be reduced.

c. The percentage scatter of the PD inception and extinction voltages is smaller than that of the breakdown voltage. This indicates that conditions in the thin helium layer where the discharges occur are more uniform than in the polymer.

d. The 38-μm D-330-DW sample appeared to be prone to surface flashovers to previous breakdown sites, even at the low breakdown voltages encountered. Visual examination of this sample revealed that the whole surface was finely scuffed as if it had been rubbed between two sheets of paper. Further tests will be made to assess the influence of surface scuffing on flashover.

The PD inception voltage data for all the samples tested so far were subjected to further analysis because of the importance of the inception voltage for cable design purposes. In general, the inception voltages increased with increasing polymer film thickness. This is a consequence of the fact that increasing the polymer film thickness decreases its capacitance, allowing it to take an increased share of the applied voltage when in series with a helium film.

The data in fact indicate that this voltage division effect is the major determinant of the inception voltage. If we treat the area under the spherical electrode as a parallel plate capacitor with a layer of helium and a layer of plastic as dielectric, the voltage is given by

$$V = E_h \left[t_h + \left(\kappa_h / \kappa_f \right) t_f \right] \tag{1}$$

where E_h, κ_h, and t_h are respectively the electric field, relative dielectric constant, and thickness of the helium layer, and κ_f and t_f similarly refer to the plastic film. Let us assume that PD inception occurs when E_h reaches the breakdown strength E_b of helium in a gap t_h. Noting that κ_h is almost exactly 1, at the inception voltage V_{inc}, we have

$$V_{inc} = V_o + E_b \left(\frac{t_f}{\kappa_f} \right) . \tag{2}$$

Hence a plot of the inception voltages vs t_f/κ_f for the various films should give a straight line of slope E_b and intercept $V_o = E_b t_h$, the breakdown voltage of the helium layer alone. Such a plot, using for t_f the actual film thickness t_a, is shown in Fig. 5, and the data do appear to be consistent with a linear dependence. A least-squares fit gives

$$E_b = 881 \text{ kV/cm}, \; V_o = 1.65 \text{ kV},$$

and t_h, the thickness of the helium layer which is discharging, is found to be

$$t_h = V_o/E_b = 18.7 \; \mu\text{m}.$$

These numbers can now be compared with the corresponding values measured for helium alone in a uniform field geometry. Measurements performed by our group[2] using sphere-plane electrodes with gaps down to 250 μm indicated that the average dc breakdown voltages with negative sphere were slightly lower than with positive sphere, and could be fitted about equally well by either of the relations

$$V_b = 43.6\ t_h^{0.78} \tag{3a}$$

or

$$V_b = 25.1\ t_h + 17.8\ t_h^{0.5}, \tag{3b}$$

for V_b in kV and t_h in mm. Using $t_h = 0.0187$ mm and dividing by $\sqrt{2}$ to convert to rms ac voltage, (3a) gives $V_b = 1.38$ kV, and (3b) gives $V_b = 2.05$ kV, in reasonable agreement with $V_o = 1.65$ kV derived from the corona measurements. Furthermore, Goldschwartz and Blaisse have performed dc breakdown measurements in boiling liquid helium down to gaps of 10 μm.[3] At a gap of 19 μm, their data give average dielectric strengths from 1170 kV/cm to 1500 kV/cm, corresponding to rms ac fields of 827 kV/cm to 1160 kV/cm. The value of $E_b = 881$ kV/cm calculated from the inception data using (2) lies toward the lower end of this range.

The agreement of the calculated inception stresses with the average helium breakdown stresses rather than the minimum values (which could easily be 50% lower at small gaps) is somewhat surprising. The probable reason is that the oscilloscope reading the capacitive divider output could not detect isolated discharges occurring at the minimum breakdown stress. More sensitive measurements using our Biddle partial discharge detector are in progress.

The above considerations indicate that the observed variations in corona inception voltage are consistent with the supposition that corona inception occurs when the stress on a thin layer of helium adjacent to the plastic film reaches the breakdown stress for the helium. The agreement of the calculated inception stresses with measured values for liquid helium indicates that the discharge is occurring in liquid rather than a bubble of helium vapor trapped under the electrode.

However, there is still considerable variation about the straight line fitted to the data, which may arise from material characteristics of the films themselves. If inception voltages for certain materials consistently lie above the line, we might conclude that they are corona inhibitors, and conversely those below the line would be corona enhancers. Investigation of Fig. 5 from this viewpoint shows the following:

a) With the exception of the 38-μ sample, all of the Nylons lie above the line.

b) Macrofol polycarbonate shows the highest percentage deviation, about 23%, above the line. Van Leer Valeron also lies considerably above the line.

c) The polyolefins all lie close to or below the line.

These observations show that the nature of the plastic film (for example, its surface roughness or chemical composition or softness and ability to conform closely to the electrodes) may have a modest effect on the corona inception voltage, apart from the value of t/κ_f.

The PD inception voltage of an actual cable will depend on its particular design characteristics. Presumably the inmost butt gaps will experience the highest stress, approximately a factor κ_f higher than the stress in the polymer. If the correlation between the helium breakdown stress in a gap equal to the butt gap thickness and the calculated butt gap stresses at PD inception also holds in multi-layer coaxial geometries, the inception stress of the cable will then be E_b/κ_f. Decreasing the butt gap thickness by using thinner tape should significantly improve the PD onset

voltage because the breakdown strength of liquid helium begins to increase rapidly when the gap decreases below about 0.5 mm.[4] Furthermore, the lower voltage across the butt gaps should decrease the energy of the discharges, reducing the possibility of PD deterioration. Of course, the tape cannot be reduced below the minimum thickness allowing sufficient mechanical strength for the wrapping process. If the cable is to be operated in a PD-free regime, it is clear that the working stress must be below E_b/κ_f, where E_b is the breakdown strength of liquid helium at the butt gap thickness. Meats has published ac breakdown strength data for helium at 5.5 K and pressures up to about 5 atm, using metal electrodes with a gap of 125 μm[5]. The breakdown field at 5 atm was found to be about 48 MV/m. If the tape used has a relative dielectric constant of 2.3, the PD inception stress is then 21 MV/m. No small-gap helium data are available for conditions in the neighborhood of 10 K and 10 atm, but data taken by Meats at 1-mm gap[6] suggest that a decrease in breakdown strength of about 25% is to be expected, reducing the inception stress to about 15 MV/m. However, Meats found[6] that the inception stress in a void between dielectric layers is higher than the breakdown stress of helium in a similar gap between metal electrodes, presumably because the dielectric suppresses field emission. Certain dielectrics may be best for suppression of PD, and further experiments to measure inception voltages in mid-dielectric voids would be useful in predicting the inception voltage of a particular cable design. It might also be possible that the relatively small area of the butt gaps would lead to higher helium breakdown stress.

2. Liquid Helium Breakdown

In order to allow a direct comparison with standard test values for conventional liquid dielectrics, the dc measurements with ASTM electrodes were repeated with ac voltage. The experiments were done with the liquid boiling slowly at 1 atm. The 80 kV transformer with a 1 MΩ current limiting resistor was used for these tests. The voltage was immediately removed upon breakdown by the Schmitt trigger circuit described in the previous quarterly report. The voltage was measured with a capacitive divider calibrated with an electrostatic voltmeter. The output was connected to an X-Y recorder to give voltage vs time. The voltage was raised by motor drive at 1.8 kV/sec. Up to 50 readings were taken at each gap. Plots of the average ac peak breakdown voltage vs gap appear in Fig. 6, along with the previous ASTM electrode measurements with negative dc voltage. In Table III, the average, minimum, maximum, and percent standard deviation are given for each gap investigated.

The first set of ac readings (closed triangles), taken from 5/16/75 to 5/20/75, agreed well with the dc readings (closed circles) at small gaps, but fell considerably below the dc values at large gaps. The electrodes had not been repolished after taking the dc data because the surface damage appeared to be minimal. However, it was decided to repolish the surface and take another set of dc and ac data, all with a single filling of helium to minimize variations in helium purity and electrode surface condition. After polishing, the edges of the electrodes were examined with a shadowgraph at 100X magnification, and it was found that the edge radius was between 25 and 50 microns. Only ten breakdowns could be taken at each gap to complete the experiment before the helium

TABLE III. Breakdown Voltages with ASTM Electrodes

	ac, 5/16-5/20, 1975*				ac, 6/5/75*				dc, 6/5/75			
(mm) d	(kV) min.	(kV) ave.	(kV) max.	%σ	(kV) min.	(kV) ave.	(kV) max.	%σ	(kV) min.	(kV) ave.	(kV) max.	%σ
1.00	13.86	15.81	17.39	5.28	16.55	20.01	23.05	8.98	17.00	18.82	19.70	3.93
2.00	20.93	24.21	26.45	4.29	29.98	38.28	43.55	9.49	26.00	31.23	34.10	9.41
2.54	23.48	26.53	29.27	4.37	40.59	48.28	50.20	5.77	31.50	39.63	43.50	10.67
3.00					41.30	45.21	51.05	7.85	35.00	47.38	50.00	11.70
4.00	33.38	35.19	37.76	3.33	46.24	52.74	63.64	9.22	41.00	48.31	55.90	12.63
5.00	37.91	40.30	43.27	3.11					47.60	55.98	64.00	8.54
6.00									46.50	62.06	71.50	11.46
7.00	43.56	47.57	51.05	3.05								
9.00	50.91	56.08	63.64	4.20								

* All ac values are peak voltage.

boiled away. The results (open triangles and circles) show much better agreement between peak ac and dc values, but both curves are now considerably higher than the first sets of dc and ac values. The later ac values are close to the standard peak ASTM breakdown voltage of C-10 transformer oil in a 2.54 mm gap (open square).

The source of these day-to-day variations in the breakdown voltage continues to be an enigma. Surface pitting by previous breakdowns does not seem to be a factor, since before repolishing the electrodes there was no evidence of a concentration of breakdown footpoints near any given pit. Surprisingly, many of the breakdown footpoints were up to several mm in from the sharp edges of the electrodes, indicating that the breakdown does not always occur at the supposed point of greatest field inhomogeneity. This may be due to field distortion by space charge collecting along the sharp edges. After completion of the measurements, the electrodes were lapped once more and again examined with the shadowgraph. No significant changes in the edge sharpness were observed. Hence the only possible effect of lapping the electrode faces between experimental runs is a general cleanup of the whole surface. Finally, the contamination level of the helium could vary. In the next quarter, further experiments will be performed to assess the effect of deliberate contamination of the helium.

C. Visitors

The following people visited us during the quarter:

April 11:	Dr. L. C. Pittenger, Lawrence Livermore Laboratory
April 17-18:	Dr. P. R. Emtage, Westinghouse Research Laboratory, Pittsburg, PA
May 29:	Dr. Tatchai Sumitra, Administrator, Nuclear Technology Program, University of Bankok, Thailand
June 9-10:	Dr. T. S. Sudarshan, National Research Council, Canada
June 17:	G. Vecsey, Swiss Institute for Nuclear Research
June 25-27:	G. L. Sommerman, Consultant

D. Personnel

Personnel associated with the Cryogenic Dielectric Program during the quarter include the following:

Dr. H. M. Long, Program Manager

Dr. S. W. Schwenterly, Assistant Program Manager

Dr. M. M. Menon, Electrical Engineer

Mr. R. H. Kernohan, Physicist

Mr. W. J. Schill, Senior Technician

Mr. G. F. Leichsenring, Mechanical Engineer

Mr. R. O. Hussung, Mechanical Engineer

Dr. G. L. Sommerman, Consultant

E. Future Plans

The major requirement for the final assembly of the high voltage cryostat is completion of the lift mechanism for the heavy dewar tanks and bushing ground plane. Construction and installation of this mechanism is expected to be completed by the end of the quarter. The final assembly and leak checking of IV3 will be carried out, and experiments will begin if no problems are encountered.

The new interwinding insulation cylinder which was completed this quarter will be installed in transformer B of the 700 kVac test set, and the coils will be reassembled. The whole transformer should be complete and remounted in the test area by the end of the quarter. It is expected that considerable care will have to be taken in removing trapped air and moisture from the coils, due to their long exposure to atmosphere.

Acceptance tests will be performed on the Universal Voltronics impulse generator, and the equipment should be received midway through the quarter. The final setup and testing will be carried out with the aid of our consultant, Dr. G. L. Sommerman.

Experiments on ac breakdown and partial discharge in polymer films will continue as new samples are received from BNL. A new test method is being considered whereby pressurized helium is injected between layers of an epoxy-enclosed multi-layer sample. Impulse tests on the films will begin as soon as the generator is received and set up. Following meetings with Dr. Chowdhuri, an appropriate program of dc polymer film breakdown experiments for LASL will be designed. Contact will also be maintained with the dielectric loss programs at NBS and Stanford, and we shall stand ready to give information and advice to or ask it from all of these programs whenever necessary. Finally, the ac breakdown work with liquid helium will be extended to the point-plane electrode geometry, and further experiments to assess the effects of contamination will be carried out.

Appendix A

DIELECTRIC STRENGTH OF LIQUID HELIUM UNDER STRONGLY INHOMOGENEOUS FIELD CONDITIONS

M. M. Menon, S. W. Schwenterly, W. F. Gauster,
R. H. Kernohan and H. M. Long

Abstract

A series of measurements has been made on the dc dielectric breakdown strength of liquid helium and other cryogenic fluids in strongly inhomogeneous field geometries. Standard ASTM electrodes and point-plane electrodes of stainless steel were used. All measurements were carried out at atmospheric pressure, with gaps up to 10 mm.

The ASTM electrode results show that the breakdown strength of liquid helium is drastically reduced below that found with sphere-plane electrodes. The breakdown strengths of liquid nitrogen and cold helium vapor were also measured, and were found to be respectively about 30% higher and 50% lower than the ASTM liquid helium results. The point-plane measurements show a strong polarity effect, with the positive polarity breakdown voltages roughly a factor of three higher than the negative voltages. Statistical analysis of the data indicates that the breakdown voltages in most cases are not normally distributed. It is concluded that strongly inhomogeneous field geometries should be avoided in the design of cryogenic high voltage equipment using liquid helium as the insulant.

REFERENCES

1. D. J. Bosack, "Development of the Dielectric System for a Helium-Cooled Superconducting Transmission Line," Proc. 1974, Conf. on El. Insulation and Diel. Phen., Dowingtown, Pa., Paper G-10.
2. ORNL-TM-4711, September 1974.
3. Low Temperatures and Electric Power, Pergamon Press, Oxford, 1970, p. 367.
4. ORNL-TM-4711, p. 24 (1974).
5. R. J. Meats, IEEE Conf. Publ. 118, 419-425 (3rd Int. Conf. on Gas Disch., London).
6. R. J. Meats, Proc. IEE 119, 760 (1972).

FIGURE CAPTIONS

1. High Voltage Cryostat with inner dewar tank mounted.
2. One test site on 125-μm Nylon 11. Magnification 100X.
3. a. Epoxy-Encapsulated Sample 2. Polymer is 100-μm Van Leer Valeron.

   b. X-ray of Epoxy-Encapsulated Sample 2.
4. Breakdown voltages, breakdown fields, and corona inception voltages of polymer film samples.
5. Plot of V_{inc} vs t_f/κ_f for polymer film samples. Numbers on points refer to Fig. 4.
6. Breakdown voltages with ASTM electrodes, using ac and dc voltages. All ac points are peak values. Slowly-boiling liquid helium at 4.2K; 1 atm.

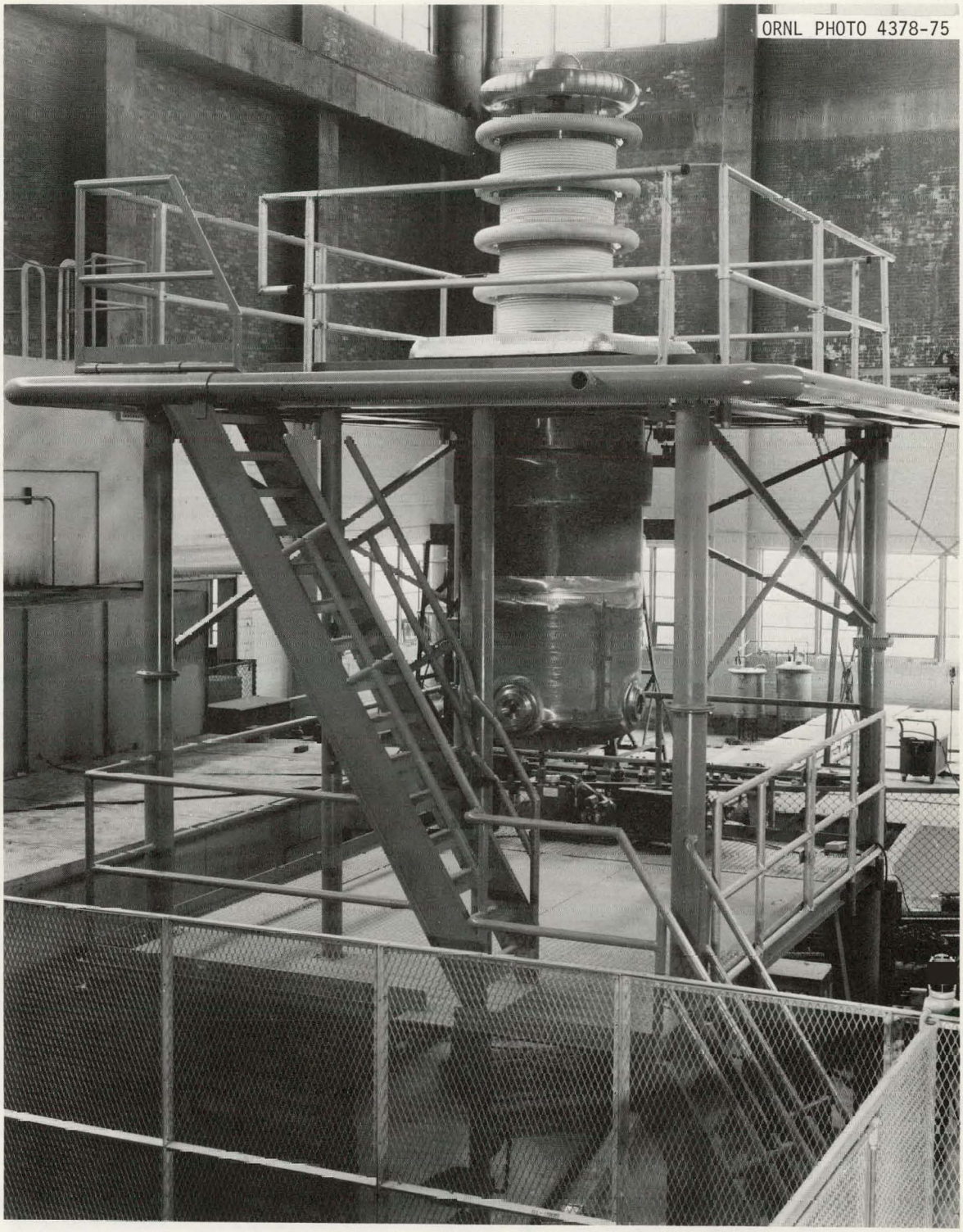

Figure 1

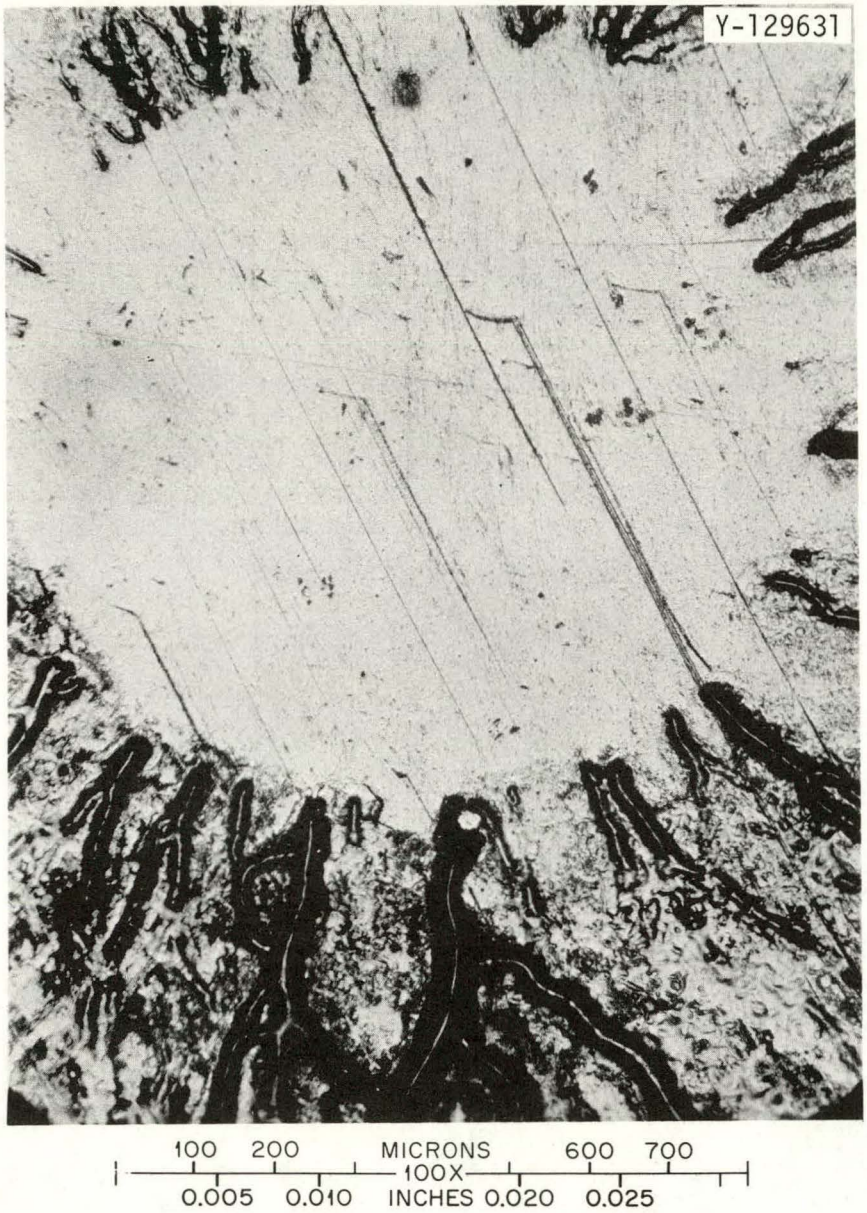
Y-129631
100 200 MICRONS 600 700
100X
0.005 0.010 INCHES 0.020 0.025

Figure 2

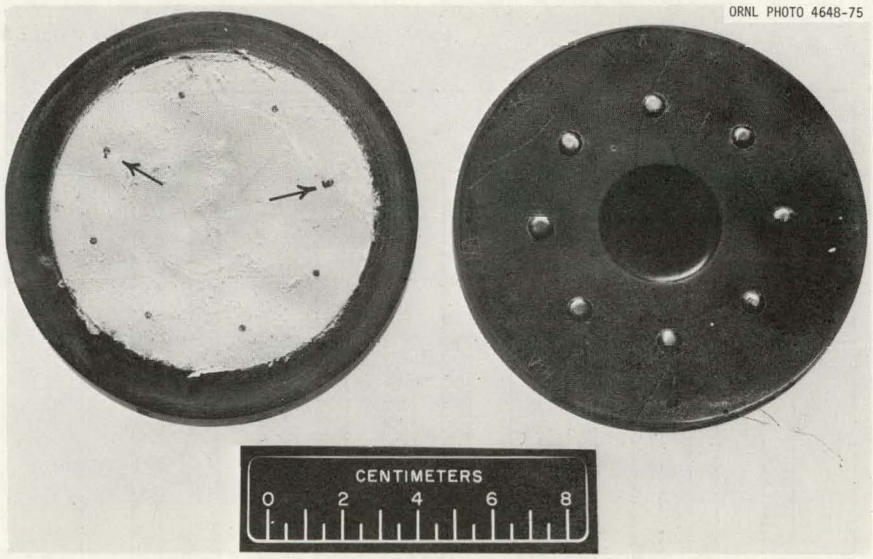

Figure 3a.

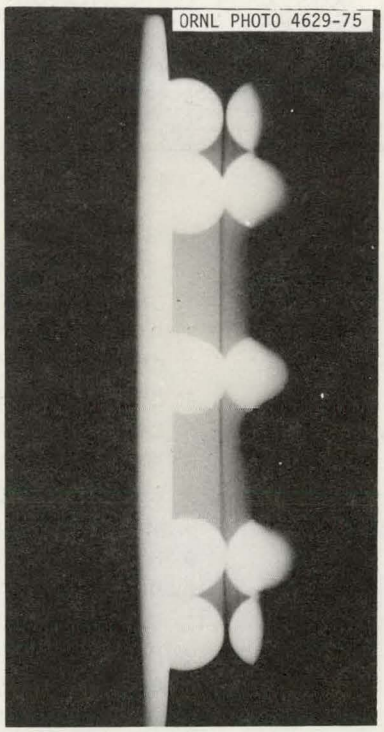

Figure 3b.

ORNL-DWG 75-12323

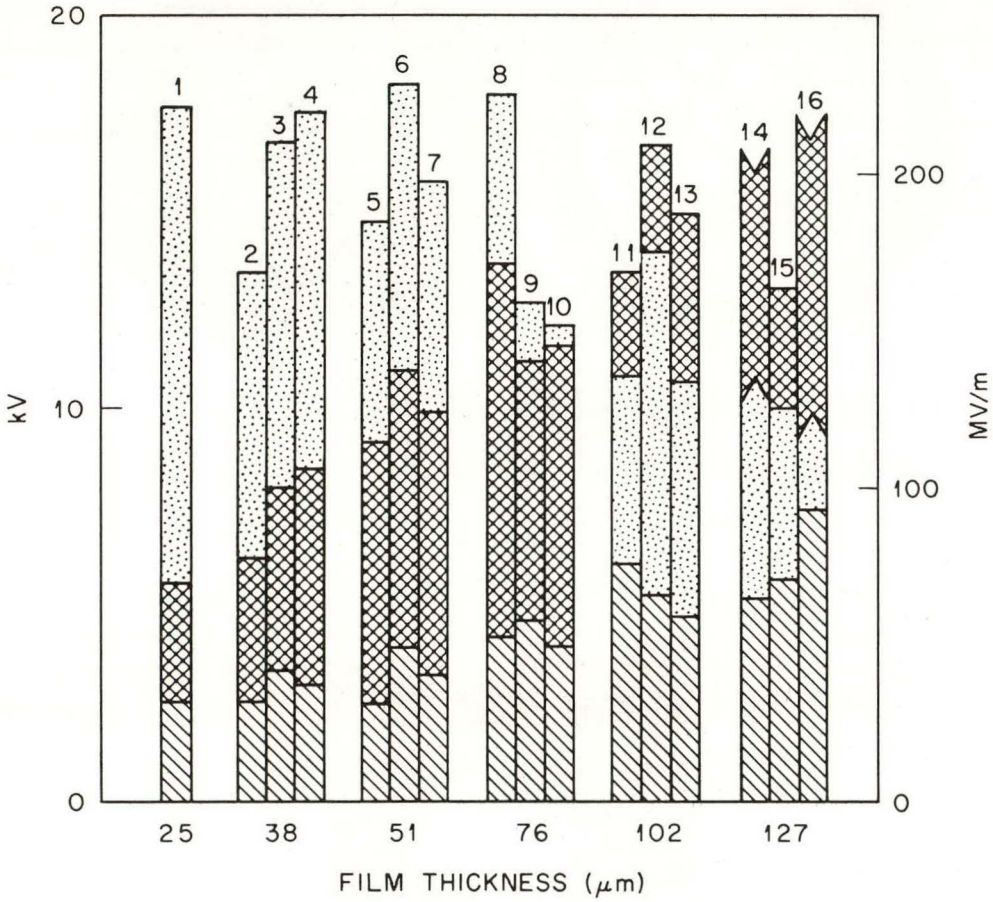

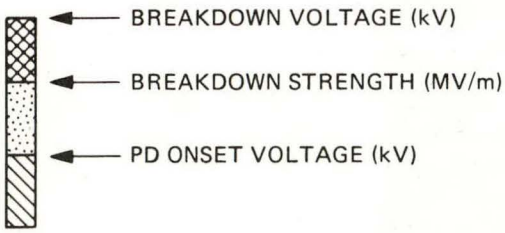

1. CRYOVAC D POLYETHYLENE
2. RYLSAN NYLON II
3. CRYOVAC D-330 DW, POLYOLEFIN
4. CRYOVAC D-330 SW, POLYOLEFIN
5. DUPONT KAPTON, 200 H
6. RYLSAN NYLON II
7. CRYOVAC BB-DYKES SILICA, POLYOLEFIN
8. MAKROFOL KG, POLYCARBONATE
9. RYLSAN NYLON II
10. DUPONT MYLAR 300 WC
11. VAN LEER VALERON, POLYETHYLENE
12. ROWLAND POLYSULFONE
13. CRYOVAC BB-DYKES SILICA, POLYOLEFIN
14. HERCULES N-400-42, POLYPROPYLENE
15. RYLSAN NYLON 12B
16. RYLSAN NYLON II

Figure 4

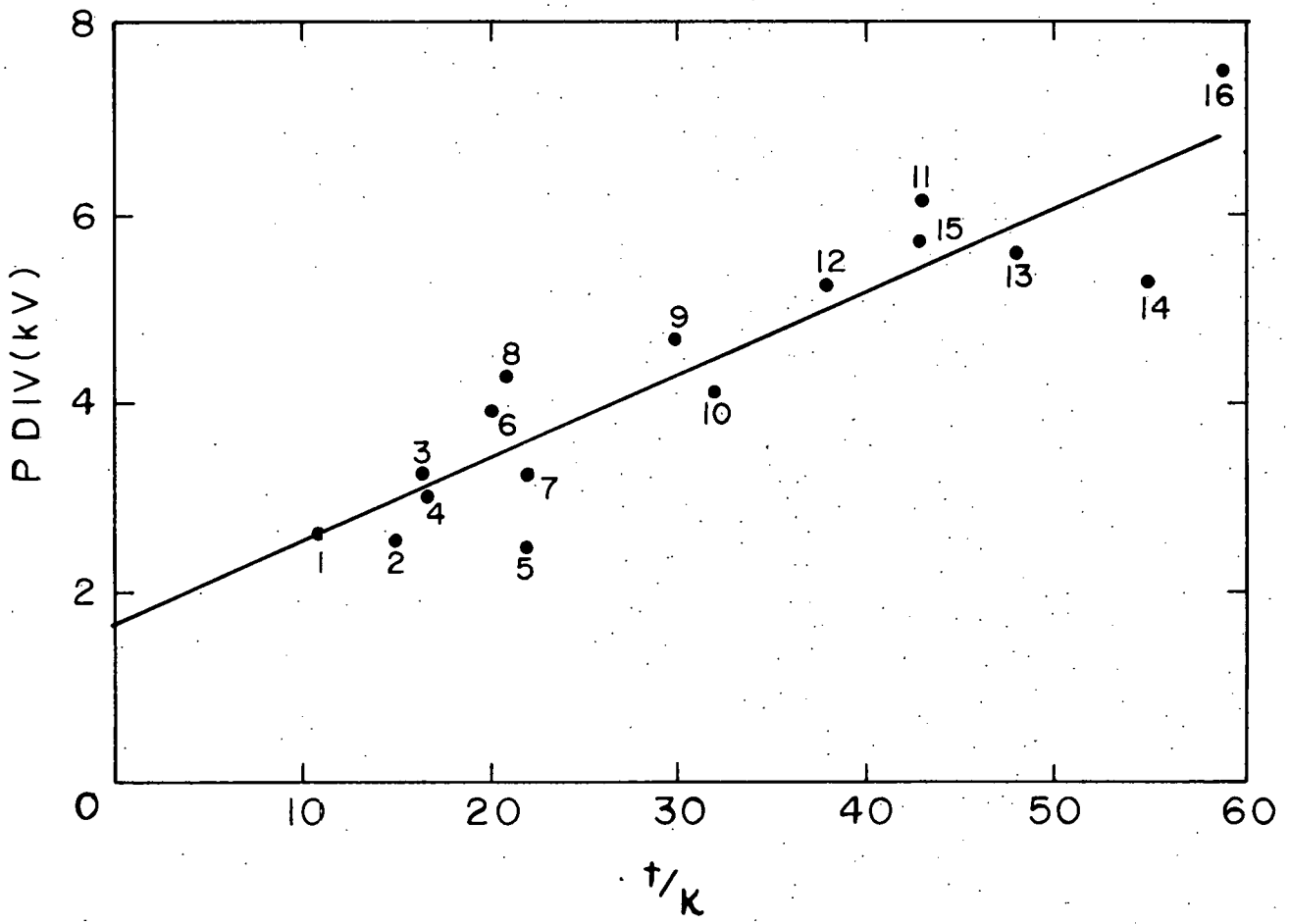

Figure 5

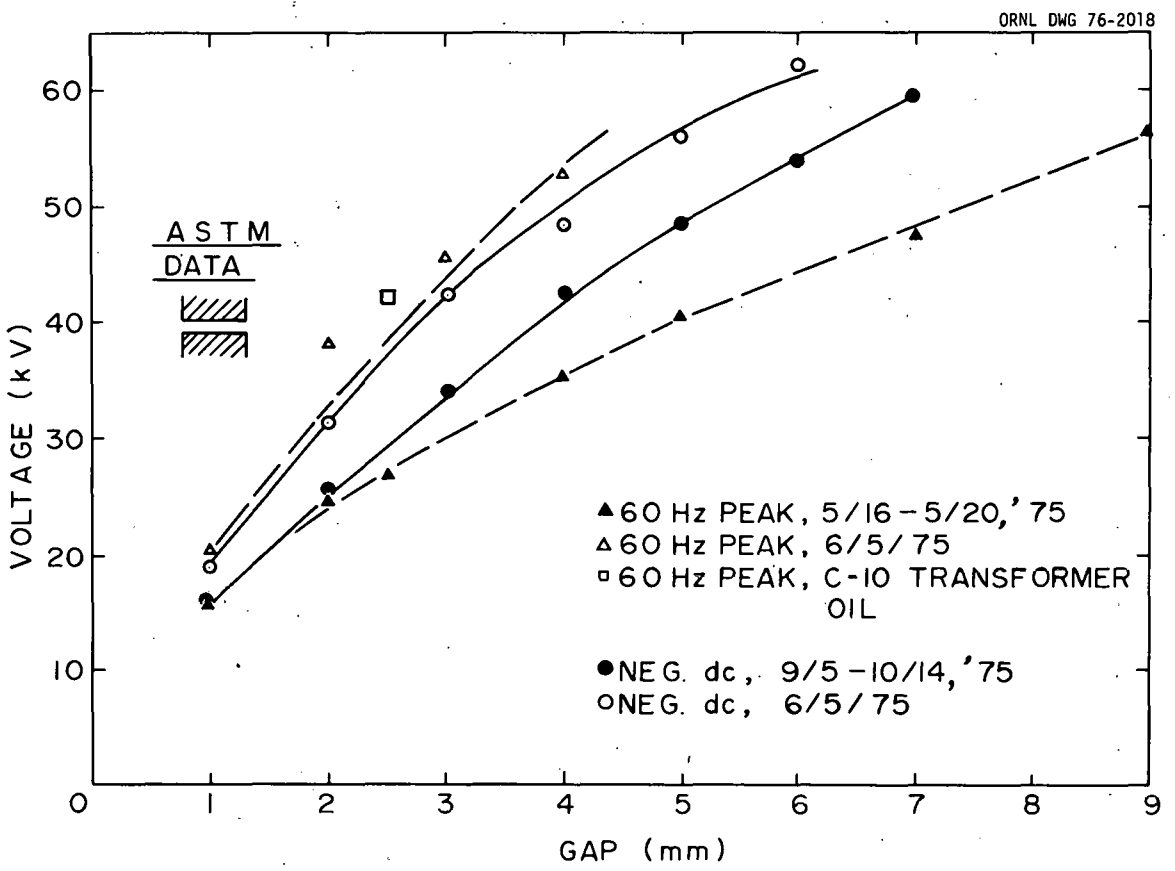
ORNL DWG 76-2018
VOLTAGE (kV)
GAP (mm)
ASTM
DATA
▲60 Hz PEAK, 5/16-5/20,'75
△60 Hz PEAK, 6/5/75
▫60 Hz PEAK, C-10 TRANSFORMER OIL
●NEG. dc, 9/5-10/14,'75
○NEG. dc, 6/5/75

Figure 6

II. AC LOSSES IN SUPERCONDUCTORS

A. Introduction

The goal of this research has been to understand the relative importance of material parameters which control ac losses in high T_c superconductors such as Nb_3Sn. This work has been in support of the Power Transmission Project at Brookhaven National Laboratory. The design of properly optimized conductors for superconducting ac transmission requires an understanding of loss mechanisms involved. That is, the essential material parameters need to be defined in order to economically fabricate a conductor with minimum ac losses.

During FY 1975 ac loss measurements were made on Nb_3Sn samples prepared by two variations of the solid state diffusion method,[1-3] and with a wide range of reaction conditions. Frequency, as well as field amplitude, was used as a parameter in the loss measurements in an attempt to more clearly define the mechanisms responsible.

The total loss per surface area per cycle was found to have the form $W_T(h_o,\nu) = W_o(h_o) + \nu F(h_o)$ where $W_o(h_o)$ is identified as a hysteretic term (i.e., frequency independent), ν is the frequency and h_o the ac field amplitude. Hysteretic losses (W_o) in the Nb_3Sn specimens were strongly dependent on the degree of surface roughness on a scale of $\sim 1\ \mu$, while the non-hysteretic losses showed only a mild dependence on the topology of the surface. This report will detail the sample preparation and characterization, the ac measurements, the results of these measurements and their interpretation. A discussion of the extraction of eddy current losses in the pickup coil is presented in Appendix I and an analysis of the ac experimental method is given in Appendix II.

B. Sample Preparation and Characterization

Nb_3Sn samples were prepared in the form of layers on 3 mm diam Nb rod ∿ 30 mm in length. As detailed in ORNL-TM-4824 (ORNL Cryogenic Power Transmission Technology—Quarterly Report, July 1—Sept. 30, 1974.), 48 different samples were prepared by the solid-state diffusion ("bronze") technique with bronze compositions of 8 wt % Sn, 11 wt % Sn, and 13 wt % Sn reacted at temperatures from 700°C to 850°C for times up to 336 hr. In addition, several samples were prepared by copper plating a Nb rod, coating with tin at 350°C, and subsequently reacting to form Nb_3Sn. After final reaction heat treatment the bronze layer was removed by a HNO_3 solution in the case of the co-deformed samples and by boiling HCl for the tin-coated samples.

The superconducting-normal transition temperatures, T_c, of the samples were measured by an inductive technique which also served as a check on the continuity of the Nb_3Sn layer. There was a general trend for higher onset temperatures and sharper transitions in samples reacted for longer times at higher temperatures. The dc magnetization measurements and estimates of J_c by two ac susceptibility techniques[4,5] were also made on selected samples. All the samples showed nearly complete flux exclusion up to fields of ∿2 kOe to the resolution of dc magnetization. The flux penetration measurements gave estimates for J_c of $\sim 2 \times 10^7$ A/cm^2 in the field range ∿1000 Oe.

Scanning electron microscopy was used to characterize the sample surfaces. The surface geometry will be discussed along with the results of the ac loss measurements.

C. ac Loss Measurements

Since the ac loss measurements are central to this work, the technique will be discussed in some detail here and in the Appendices.

The measurement of ac losses was done electronically in a manner similar to that developed by Sekula[6] in which a tuned lock-in amplifier is used to examine that component of the voltage, induced in a pick-up coil wound around the sample, in phase with and at the same frequency as the applied ac magnetic field. In our method, however, no steady dc magnetic field is present and the ac field oscillates over the range $-h_o \leq h \leq +h_o$ while at the same time h_o itself is slowly varied. The mean power loss per unit cylindrical surface area is given by:

$$\bar{p} = \frac{1}{2\pi R\tau} \int_0^{\tau} h \frac{d\phi_s}{dt} dt \qquad (1)$$

where R is the radius of the sample, h is the applied ac magnetic field of period τ and ϕ_s is the flux contained within the sample. For sinusoidal h(t), this can be rewritten as an energy loss per unit surface area per cycle in the following way,

$$W = 0.127 \frac{\langle h\rangle\langle v\rangle}{NR\nu} \qquad (2)$$

where $\langle h\rangle$ is the rms field in Oersteds, $\langle v\rangle$ is the rms voltage as registered by the lock-in amplifier in volts, N is the number of turns in the pick-up coil, ν is the frequency of the applied magnetic field in Hertz and R is the specimen radius in cm. Using these units for the measurable quantities yields a W that is in units of Joule cm^{-2} $cycle^{-1}$.

The output of the lock-in amplifier drives the Y-axis of an X-Y recorder while the X-axis is driven by a voltage proportional to the rms current flowing in the field producing solenoid. In this manner, a sweep of h at a fixed frequency produces a response v(h) and only the product of these two quantities is needed via Eq. (2) to determine the surface loss per cycle.

The solenoid used to produce the ac field is a copper coil wound from Litz wire and is situated directly in the helium bath. Copper windings were chosen after initial work with superconducting wires, both single and multifilament, indicated complications due to intrinsic losses in these materials. Test runs on dummy micarta samples revealed spurious losses which were eliminated by removing all extraneous metal (e.g., solder joints) from the vicinity of the sample and pick-up coil.

Compensation of the unwanted signal due to changes of flux between the pick-up coil and the sample was achieved by means of a coil of a few turns located in the fringing field of the copper solenoid and connected in opposition to the sample coil. Complete cancellation of total signal was achieved in fields typically of a few Oersted by mechanically adjusting the location of the sample pick-up and compensating coils within the bore of the solenoids. This condition was checked after each field sweep to insure that compensation was maintained throughout the data gathering period. This method of compensation used in conjunction with a lock-in amplifier having an input impedance of $\sim 10^7 \Omega$ avoided the possibility of unwanted phase shifts being introduced electronically while at the same time maintaining the sample and its pick-up coil

within the uniform field region of the solenoid. The reference phase of the lock-in was established by nulling the signal induced in the compensator coil (i.e., set to examine any signal in phase with the applied ac magnetic field). This procedure was repeated before any field sweep was taken following a change of operating frequency.

The sensitivity of this method is ideally limited by the ability of the lock-in amplifier to extract the signal of interest from the attendant noise. It should be noted, however, the $\langle v \rangle$ may contain contributions from sources external to the superconductor and, therefore, an uncritical use of Eq. (2) may give rise to an erroneous value for the loss per area per cycle, W. Our apparatus was able to reliably detect losses of the order 10^{-9} Joule cm^{-2} $cycle^{-1}$.

The ac loss measurements were made on a number of selected Nb_3Sn samples. However, our detailed analysis concentrated on two extreme cases--a "low" and a "high" loss sample. The other samples had intermediate loss values and exhibited no anomalous behavior. The "low" loss sample was prepared by co-deformation of Nb in a Cu-10 wt % Sn alloy and reaction for 42 hours at 800°C. The "high" loss sample was prepared by the tin coating process described above with a reaction heat treatment of 48 hours at 800°C. The similar final reaction treatment produced similar onset T_c values for the "low" and "high" loss sample of 17.83K and 17.78K, respectively, although the "high" loss sample exhibited a broader transition width (∿2.5K) compared to the "low" loss sample (∿0.3K).

To help validate the measuring technique and elucidate the loss mechanisms, ac losses were also measured on a Mo-25 at % Re alloy sample and on a Nb single crystal sample.

D. Results

First, results on ac losses in Mo-25 at % Re are presented to give evidence for the validity of the measuring technique and illustrate a material in which the ac losses are overwhelmingly hysteretic in nature. Then a discussion of the eddy losses from the copper pick-up coil is given with the method used to extract it from the losses in the superconductor. Finally, the loss data on the Nb_3Sn and Nb samples are presented.

1. Mo-25 Re

Flux enters the bulk of Mo-25 Re at a relatively low field ($H_{C_1} \approx 450$ Oe) and the losses above this value appear to be purely hysteretic in nature. The criterion used throughout this paper is to assume that any loss per cycle which is independent of frequency is, in fact, hysteretic. At high field amplitudes such as, for example, 1456 Oe, the induced signal $\langle v \rangle$ varies linearly with frequency yielding $\langle v \rangle = 5.22 \times 10^{-4} \nu$. This, in turn, produces a W_o of 1.68×10^{-3} Joule cm^{-2} $cycle^{-1}$ constant over the frequency range examined (40 to 100 Hz). While there was no obvious dependence of W on frequency at any field levels, it should be noted that at lower field amplitudes there is some scatter in the results due to variations in the previous magnetic history of the sample. The losses from hysteresis loops obtained by dc magnetization and the ac losses are in good agreement over much of

the mixed state region examined. Fig. 1 is a B versus H (dc) trace in which the external field was varied between ±756 Oe. The total loop was symmetric and so for simplicity only half of it is shown in the figure. Fig. 2 shows the surface loss per cycle determined as a function of peak magnetic field for both ac and dc conditions. The dc data shown for four field values are in agreement at the lower two values where the induced voltage waveform taken directly from the pick-up coil can be shown to qualitatively yield B versus H responses as shown in Fig. 1. For peak fields in excess of 1200 Oe, the losses determined via the ac technique increase linearly with the value of the peak field. This is revealed as a saturation of the induced voltage signal with field at a fixed frequency. It is interesting to note that this is the behavior predicted for such losses by the Bean model when $H_{peak} > H^*$ (the so-called filling field).

The ac losses in Mo-25 Re at low fields depend critically on the magnetic history of the sample. Having cycled the Mo-25 Re well into the mixed state ($h_o \sim 1400$ Oe) and subsequently measured the losses at low fields, one finds that the loss at a given field value can be as much as a factor of twenty greater than in the virgin sample.[7] Fig. 3 shows the normalized difference, $(W_2-W_1)/W_2$ referred to as the loss enhancement factor, as a function of peak ac field, W_1 being the loss in the virgin sample and W_2 being the loss at the same field and frequency but after a field excursion well into the mixed state. A rapid drop in this quantity begins at about 600 Oe, that field value at which the dc magnetization indicates $dM/dH \approx 0$ (not at H_{C_1}). This would seem to

indicate that in bulk hysteretic materials one must achieve a field amplitude at which a certain threshold amount of flux penetrates the sample and not simply H_{fp}, the field of first penetration, before the losses become independent of previous magnetic history.

2. Eddy Losses in Copper Pick-Up Coil

The loss response of the high-loss Nb_3Sn sample was examined in detail with two pick-up coils wound from copper wire of different diameter in separate experiments. By so doing we were able to extract the eddy-loss contribution of the pick-up coil from the total measured loss.

The rms voltage signals for the two cases can be represented as follows:

$$\langle\varepsilon_1\rangle = S_1 + A_1$$

and $$\langle\varepsilon_2\rangle = S_2 + A_2$$

where S_1 and S_2 are the voltage signals from the superconductor while A_1 and A_2 are those arising from within the pick-up coils themselves. $\langle\varepsilon_2\rangle$ can be rewritten, normalizing it with respect to $\langle\varepsilon_1\rangle$ as follows:

$$\langle\varepsilon_2\rangle = \frac{N_2}{N_1} S_1 + \frac{N_2}{N_1}\left(\frac{a_2}{a_1}\right)^3 A_1$$

where $N_{1,2}$ refers to the number of turns on the respective coils and $a_{1,2}$ to the respective radii of the wires used. Thus:

$$S_1 = \frac{\left(\frac{a_2}{a_1}\right)^3 \langle\varepsilon_1\rangle - \frac{N_1}{N_2}\langle\varepsilon_2\rangle}{\left(\frac{a_2}{a_1}\right)^3 - 1} \quad \text{and} \quad A_1 = \frac{\frac{N_1}{N_2}\langle\varepsilon_2\rangle - \langle\varepsilon_1\rangle}{\left(\frac{a_2}{a_1}\right)^3 - 1}.$$

In our cases,

$$N_1 = 325,\ N_2 = 151,\ a_1 = 2.5 \times 10^{-3}\ \text{cm and } a_2 = 6.4 \times 10^{-3}\ \text{cm},$$

and therefore, $S_1 = 1.068 \langle\varepsilon_1\rangle - 0.147 \langle\varepsilon_2\rangle$ for a given h_o and ν. Examining this at 165 Oe and 200 Hz we find $\langle\varepsilon_1\rangle \approx 4.0\ \mu V$ and $\langle\varepsilon_2\rangle \approx 7.5\ \mu V$ yielding $S_1 \approx 3.2\ \mu V$ and $A_1 \approx 0.8\ \mu V$. This value for A_1 compares favorably with our approximative first principles calculation of $\sim 0.4\ \mu V$ -- see Appendix I.

Next, the data of the two runs were examined to determine the loss per unit area per cycle associated with the copper voltage signal as a function of field amplitude h_o at a fixed frequency of 200 Hz. The results of this are shown in Fig. 4. It is to be noted that W_{Cu} displays the expected h_o^2 dependence associated with eddy behavior. Fig. 5 shows the copper signal at 500 Hz versus that at 200 Hz for the same field values. The slope is about 6.10 and that expected on the basis of eddy behavior is 6.25. These results taken together provide confirmation of the existence of eddy-current voltages in the copper pick-up coil which in turn give rise to an apparent W. In the subsequent reduction of our data we have taken the experimentally determined relations for

$\langle\varepsilon_{Cu}\rangle$ and W_{Cu}, i.e.

$$\langle\varepsilon_{Cu}\rangle = 1.81 \times 10^{-15}\ \frac{NR}{\rho}\ a^3\nu^2 h_o \text{ volts}$$

and $$W_{Cu} = 1.67 \times 10^{-16}\ h_o^2\nu \text{ Joule cm}^{-2} \text{ cycle}^{-1}.$$

3. Nb and Nb_3Sn

The ac loss behavior of the niobium single crystal and the low-loss Nb_3Sn sample was markedly different from that of the Mo-25 Re and could be represented by $W_T(h_o,\nu) = W_o(h_o)+\nu F(h_o)$ where $W_o(h_o)$ is the hysteretic loss per area per cycle and $F(h_o)$ represents the field dependence of the frequency dependent contribution. Fig. 6 is a dc magnetization curve of the Nb single crystal while Fig. 7a reveals the total loss per area per cycle of the niobium as a function of frequency for various values of the amplitudes of the ac field. Two things should be noted: (1) the linear dependence of the loss per cycle on frequency, and (2) the fact that the losses decrease to very small values at zero frequency (i.e., $W_o \leq 5 \times 10^{-9}$ Joules cm^{-2} $cycle^{-1}$). This is to be compared with the work of Rocher and Septfonds[8] who found a slight linear dependence of the loss per cycle on frequency in niobium and also a hysteretic loss in fields as low as 90 Oe. Their method of measurement was a calorimetric one and so avoided any problems associated with the loss behavior of pick-up coils. The low-loss Nb_3Sn exhibits a similar response as shown in Fig. 7b but with the distinction that in this case a measurable hysteretic contribution (finite W as $\nu \to 0$) is in evidence which increases rapidly with field amplitude.

Fig. 8 shows the hysteretic loss per cycle W_o in the low and high-loss Nb_3Sn. The latter reveals an h^3 dependence over the field range investigated. The hysteretic loss per cycle in the low-loss Nb_3Sn is at least two orders of magnitude less than for the high-loss material at fields $\lesssim$ 1 kOe.

Fig. 9 shows $F(h_o)$ versus h_o^2 for the two Nb_3Sn samples and the single crystal niobium. The low-loss Nb_3Sn reveals a departure from h_o^2 only at the highest fields tested while the high-loss Nb_3Sn appears to depart from h_o^2 behavior at even the lowest fields examined. $F(h_o)$ for our single crystal niobium shows a departure from h_o^2 dependence occurring at a field value intermediate between the two Nb_3Sn samples.

Losses measured in the single crystal Nb and Nb_3Sn show very little dependence on previous magnetic cycling in fields up to 1400 Oe. Thus there should be little ambiguity in the magnitude of such losses between various experiments in contrast to the results on Mo-25 Re and other such alloys.

E. Discussion

Losses in all the samples we examined (including the Mo-25 Re) begin to appear at very low fields and a word concerning this aspect of the response is in order here. There are two factors working toward finite losses in small fields and both arise from the departure of the sample surface from ideal planar geometry. First, the demagnetization factor D associated with pseudo-ellipsoidal protuberances leads to the onset of the mixed state within these regions at a field value of $(1-D)H_{C_1}$ where H_{C_1} is the bulk lower critical field.[9-11] Second, there is the phenomenon of field enhancement in the vicinity of these surface irregularities. Melville[12] has discussed this effect in analogy to the electric field enhancement known to occur from studies on field emission and electrical breakdown. If γ is the enhancement factor of a magnetic field applied parallel to the overall surface near a projection, then the field amplitude

h_o need only take on the value $(1-D)H_{C_1}/\gamma$ in order that fluxoids enter regions of surface irregularity. Plausible values of D and γ lead one to expect such establishment in applied field amplitudes significantly reduced from H_{C_1}.

1. Mo-25 Re

Various models for hysteretic losses predict a dependence on magnetic field of h_o^n where $n \geq 3$ (Ref. 29-32). Our results on Mo-25 Re indeed display a cubic dependence on h_o at the lowest fields providing that the sample has not undergone excursions to high fields with subsequent flux trapping. This type of loss dependence on h_o is typical of hysteretic losses and is predicted by the Bean model for low fields (i.e., $h_o \ll H^*$, the "filling field"). The extremely rapid increase of W with h_o over the range from 600 to 900 Oe makes it very difficult to compare results between various researchers on such alloy superconductors (aside from complications due to different magnetic histories). To fit our data in this relatively small field region to $W \propto h_o^n$ would yield a value of n between 10 and 12.

While there is reasonable agreement between ac and dc determined losses in Mo-25% Re at fields where such losses are not influenced by previous history, we do not have an explanation for the observed differences measured for the losses at fields in excess of 1 kOe. Earlier work conducted by Linford and Rhodes[13] on hysteretic losses determined via ac and dc methods reveals much the same degree of agreement as we find in this work. An inspection of the waveform of the signal induced in the compensated pick-up coil at these fields does indeed indicate a

greater degree of flux exclusion in increasing field which in turn gives rise to a larger ac loop and a greater loss than the corresponding hysteresis loop taken from the dc magnetization studies. The additional losses may be due to bulk viscous effects in the Mo-25 % Re as these fields are well in excess of H_{C_1}, but more detailed work needs to be done to clarify this, particularly since the ac losses here appear to be independent of frequency, at least over the narrow range (40 to 100 Hz) which could be achieved in this work at these higher fields. As we have often seen, measurements need to be taken over a significant range of frequencies to avoid misinterpreting possible scatter in data.

Irie *et al*[14] have examined the field and frequency behavior of ac losses in Nb-50 Ta at field amplitudes up to H_{C_1} ~60 Oe at 4.2K and for $0.5 \lesssim \nu \lesssim 18$kHz. This system can be expected to behave similarly to our Mo-25 Re, both materials exhibiting relatively low pinning. Irie *et al* find losses per cycle varying at h_o^3 in fields less than H_{C_1} with an extreme increase in the dependence of W_o on h_o occurring near H_{C_1}. In addition, while they do find losses per cycle varying with frequency, these are seen to occur only at frequencies $\gtrsim$ 500 Hz. For frequencies $\lesssim$ 500 Hz only hysteretic losses can be resolved from their data. Our data taken up to 500 Hz are consistent with these results. The field and frequency response of both materials are qualitatively similar and may be representative of superconductors where the dominant loss mechanism is hysteretic.

2. Nb and Nb_3Sn - Hysteretic Losses

Fig. 10 consists of six scanning electron micrographs taken of the Nb and two Nb_3Sn specimens. For each sample, two micrographs are presented, one perpendicular to the specimen surface and one viewing its edge profile. The high-loss Nb_3Sn (Figs. 10a and b) has a rough surface structure on the scale of a micron. The low-loss Nb_3Sn (Figs. 10c and d) and the single crystal niobium (Figs. 10e and f) have much smoother surfaces than the high-loss Nb_3Sn with the low-loss Nb_3Sn showing somewhat less structure on a scale of the order of a micron than that of the single crystal Nb. The ridges and depressions in both the low-loss Nb_3Sn and the single crystal Nb are predominantly aligned in a direction parallel to the axis of the cylindrical sample and therefore parallel to the applied magnetic field.

Hysteretic losses per cycle, if present in our single crystal Nb sample, must be less than the order of 5×10^{-9} Joules cm^{-2} $cycle^{-1}$ in fields approaching H_{C_1} (see Fig. 7a). This is compatible with the extremely smooth surface of the Nb specimen as seen in the micrographs (Figs. 10e and f) and the correspondingly small values of γ and D.

The hysteretic loss per cycle of the high-loss Nb_3Sn has an h_o^3 dependence over the field range investigated (Fig. 8) for which the Bean model predicts a critical current density of:

$$J_c = \frac{5 \times 10^{-7}}{12\pi^2} \left(\frac{h_o^3}{W_o}\right) A\ cm^{-2}$$

which for our case yields a value of $J_c = 6.6 \times 10^6$ amp.cm^{-2} for $165 \leq h_o \leq 1324$ Oe. While the Bean model can be used to calculate a uniform J_c whenever $W_o \propto h_o^3$ it is not apparent that such a J_c should be associated with the actual coarse structure seen at the surface of our high-loss Nb_3Sn sample. More to the point in this case is the prediction of Melville[12] for losses occurring in surface irregularities. Melville has shown that the hysteretic loss per cycle per unit surface area is related to the field amplitude by $W_o \propto h_o^{u+2}$ where u is characteristic of the shape of the surface irregularities. In our case, a scanning electron micrograph taken of the surface at 10^4X magnification reveals the contours of the irregularities to be best approximated by a series of straight line segments which can in turn be represented by some average slope. For such a case, the parameter u (called w in Melville's paper) assumes the value of unity and $W_o \propto h_o^3$. Melville's estimated magnitude of loss for u = 1 is about $(0.2 - 6) \times 10^{-7}$ Joules cm^{-2} cycle^{-1} at a field of $\sim$ 1000 Oe. This is in good agreement with our measured value of 6.5×10^{-7} Joules cm^{-2} cycle^{-1} at this field.

The low-loss Nb_3Sn has a much smoother surface on a scale of the order of $\sim$1 μm and thus correspondingly reduced enhancement and demagnetization factors. The result is a higher degree of flux exclusion from the surface in the lowest fields, and due to a very large J_c, a high degree of flux exclusion from the bulk even in fields somewhat in excess of H_{C_1}, yielding lower losses per cycle but also an extremely strong dependence of W_o on field amplitude once flux enters. This would seem to indicate that at higher fields the hysteretic losses per area per cycle of the low and high loss samples of Nb_3Sn may become comparable,

as one might expect once the loss mechanism becomes characterized by the bulk response of the superconductor. In general, the hysteretic loss contribution appears strongly correlated to the physical nature of the surface in the Nb and Nb_3Sn cases.

3. Nb and Nb_3Sn - Non-Hysteretic Losses

The frequency dependent losses per surface area per cycle are characterized by $\nu F(h_o)$ reflecting the fact that in all cases any variation of W_T with frequency was found to be a linear one. Fig. 9 shows $F(h_o)$ versus h_o^2. It was found that the initial variation with h_o was quadratic up to a certain field h_o^*. The low-loss Nb_3Sn has an h_o^* of about 1200 Oe while the value associated with the single crystal Nb is about 930 Oe. The high-loss Nb_3Sn departs from an h_o^2 variation at very low fields making it difficult to assign a value of h_o^*. As can be seen in Fig. 9 the magnitudes of $F(h_o)$ for the three samples at a given applied field are only slightly different (about a factor of 5 at 1200 Oe). There appears, however, to be a stronger correlation of h_o^* with surface condition although the reason for this is not understood at present.

Normal excitations scattering near the specimen surface would yield a $W \propto \nu$ and, assuming a layer of fixed depth from which these "electrons" originate, a dependence for h_o of $W \propto h_o^2$. In fact, the Nb and low-loss Nb_3Sn showing only slight departure from ideal geometry on a scale of the order of a micron display an initial quadratic field dependence up to 900 Oe and 1200 Oe, respectively. In this regard, it is of interest to note that Campbell technique[15] measurements of flux gradients in some

superconductors reveal an absence of any gradient within a region located at the surface. Tunneling experiments[16] have also indicated the possibility of normal material within a coherence length of the surface.

The possibility also exists that the frequency dependent term arises from fluxoid motion. The degree of surface smoothness of the Nb and low-loss Nb_3Sn specimens would seem to mitigate against this, especially in the case of the Nb from which $H_{C_1} \cong 1275$ Oe. Kramer,[17] however, has postulated that in the process of vortex formation there is a stage at which nascent vortices first broaden to form a normal layer at the surface from which Abrikosov vortices subsequently nucleate.

Thus, there are in fact a number of independent studies which have suggested the possible existence of a normal-like region in the immediate vicinity of the surface. Certainly ac losses, in those superconductors for which such processes are confined to the neighborhood of the surface, should be expected to be extremely sensitive to such a layer.

Table I illustrates the contributions of W_o and $W(\nu) \equiv \nu F(h_o)$ to the total loss per area per cycle occurring in the listed superconductors at a frequency of 60 Hz and a field amplitude of 745 Oe. It is to be noted in passing that if a detailed frequency dependence were not made, and if no correction were made for losses in the copper pick-up coil, the loss value assigned as being totally hysteretic would be an overestimate of the actual W_o. For example, at $\nu = 60$ Hz and $h_o = 890$ Oe,

$$\frac{W_o}{W_o + W(Cu) + W(\nu)} \approx 0.272 \text{ and not unity.}$$ This points out

the need for examination of the frequency response of ac losses and careful analysis of whatever experimental method is used in order to properly identify the contributions to the total apparent loss and to assign correct values to their magnitudes.

F. Summary and Conclusions

Losses per surface area per cycle in all materials examined were of the form $W_T(h_o,\nu) = W_o(h_o) + \nu\, F(h_o)$. Extensive examination of the frequency dependence of the losses was necessary in order to correctly identify the hysteretic loss contribution $W_o(h_o)$. Elimination of the eddy signal induced in the copper pick-up coil allowed a determination of any frequency dependent loss per cycle occurring in the superconductor.

The Mo-25 Re, used primarily to provide a method of checking our method of ac loss determination against the dc case, revealed no resolvable frequency dependent contribution to W. Its response may be representative of that associated with weakly pinned superconductors in which flux can penetrate well into the bulk sample during a field cycle. In this case, the large hysteretic losses mask any frequency dependent contribution.

Nb_3Sn prepared by the solid state diffusion technique (low-loss sample) exhibited only small hysteretic losses ($W_o \lesssim 7 \times 10^{-9}$ Joules cm^{-2} $cycle^{-1}$) for fields below about 950 Oe. The small hysteretic loss per cycle for fields well in excess of H_{C_1} appears to be the result of an extremely large critical current density ($J_c \approx 2 \times 10^7$ amp cm^{-2} at $\sim$1000 Oe) associated with this specimen with consequent little flux penetration. A small but measurable frequency dependent term was observed at all fields for which $F(h_o) \propto h_o^2$ up to about 1200 Oe.

Single crystal Nb showed small hysteretic losses, ($W_o \lesssim 5 \times 10^{-9}$ Joules cm^{-2} $cycle^{-1}$) for fields up to about H_{C_1} (1275 Oe). A frequency dependent term somewhat larger than that of the low-loss Nb_3Sn was observed, however, having $F(h_o) \propto h_o^2$ up to about 900 Oe and then varying more strongly with h_o for higher fields.

The "high-loss" Nb_3Sn sample had both large hysteretic and non-hysteretic loss contributions. A hysteretic loss per area per cycle varying as h_o^3 was observed across the field range examined (100-1300 Oe) and a frequency dependent term was revealed whose $F(h_o)$ departed from quadratic dependence at fields of the order of 100-200 Oe. The hysteretic term appeared to be that predicted by Melville[12] for rectilinear surface irregularities.

While the magnitude of the hysteretic losses appears to be strongly correlated with the degree of surface roughness on a scale of the order of a micron, the same is not the case for the frequency dependent contribution to the total loss per area per cycle.

G. Personnel

Personnel associated with the ac Losses Program during the quarter include the following:

Dr. C. C. Koch, Group Leader

Dr. D. J. Griffiths, Oregon State University, Physicist

Mr. Paul Jones, Technician

Appendix A

Eddy Signal from the Pickup Coil

The experimental method of ac loss determination in which a pick-up coil is wound on the sample and in which an ac magnetic field is produced at the site of the sample by means of an external solenoid, merits a careful analysis of the observed induced voltage signal. For pure sinusoidal applied magnetic fields, the mean loss per cycle is determined by the component of the induced voltage having the same frequency as and being in phase with the applied magnetic field.

The method used in our experiments allows an isolation and examination of this component by means of lock-in techniques using phase sensitive detection. Nevertheless, there will be a contribution to this component of the induced voltage due to eddy-currents set up in the pick-up coil itself. The following is a calculation of the order of magnitude of such signals expected to appear in general and in our experiments in particular.

Consider a single layer coil of N turns wound on a sample of radius R, the wire itself being of radius a. The peak induced voltage ε_o in phase with the applied field is given by $\varepsilon_o = 8\pi^2 NRa\nu\mu'' h_o$ where ν is the frequency of h(t), μ'' is the imaginary part of the permeability of the copper under application of h(t) and h_o is the magnitude of h(t). Here we have assumed that a << R. In general, $b_o = (\mu' - i\mu'')h_o$ where the real and imaginary part of the permeability are taken to be those given by Landau and Lifshitz[18] for an infinite cylinder of radius a situated in a transverse ac magnetic field. Our geometry approximates this case quite well since R >> a.

In the limit of $\delta >> a$ where δ is the skin depth (a condition also well met in our case) one can write:

$$\mu' = \mu_o \left[1 - \frac{1}{24\pi}\left(\frac{a}{\delta}\right)^4\right] \approx \mu_o$$

and $$\mu'' = \frac{\mu_o}{8\pi}\left(\frac{a}{\delta}\right)^2 \text{ where } \mu_o = 4\pi \times 10^{-7} .$$

Substituting for the skin depth its usual expression and converting from MKS units to those of experimental convenience, we arrive at the form for the RMS value of the eddy signal, $\langle\varepsilon\rangle = 8.77 \times 10^{-16} \frac{NR}{\rho} a^3 \nu^2 h_o$ volts where R and a are in cm, ρ in $\Omega\cdot$ cm, h_o in Oersted and ν in Hz. For the actual parameters occurring in our experiments this yields a value of $\langle\varepsilon\rangle \cong 0.4\ \mu\nu$ at a field amplitude of 165 Oe and a frequency of 200 Hz.

Appendix B

Analysis of the Experimental Method

Consider the applied ac magnetic field to be represented by $h(t) = h_o e^{i\omega t}$. We can then represent the response of the induction as follows: $b_o = \mu'_i h_o$ in the helium space interior to the copper windings of the coils and $b_o = (\mu' - i\mu'')h_o$ within the windings themselves. If no flux penetrates the superconductor (a good approximation in fields of a few Oe where the compensation condition is set) then the compensated signal is given by:

$\varepsilon = N_c \frac{d\phi_p}{dt}$ where N_c, N_p are the number of turns of the compensator and pick-up coils respectively, and ϕ_c, ϕ_p refer to the flux threading the compensator and pick-up coils respectively, both within their enclosed areas and within the actual windings. In terms of the peak induced signal ε_o, we have:

$$\varepsilon_o = 2\pi d\ (N_p R_p - N_c R_c \eta)\ \mu'' \omega h_o + i\pi\{2N_p[R_s \Delta R \mu'_i + R_p d\mu'] - \eta N_c R_c (R_c \mu'_i + 2d\mu')\}\omega h_o$$

where R_p, R_c, R_s are the radii of the pick-up coil, compensatng coil and sample respectively, ΔR is the mean difference between R_p and R_s, d is the effective thickness of the wire assumed to be the same for both pick-up and compensator windings, ω is the angular frequency of the magnetic field, η is the fractional value of the field at the location of the compensating coil relative to the field value at the location of the sample. The compensation of the induced signal in phase with $\frac{dh}{dt}$ is achieved by mechanically adjusting the former on which the coils are

wound as described in the text since obviously $\eta = \eta(x)$. Proper compensation then means that the imaginary term in the above expression for ε_o is zero which yields for $\Delta R \ll R_s$, $\eta(x) = \frac{2N_p R_s}{N_c R_c}\left(\frac{\Delta R + d}{R_c + 2d}\right)$ independent of h_o. At the low frequencies examined here it is well justified to take $\mu_i' \approx \mu' \approx \mu_o$. Even at proper compensation, however, there will be a non-zero real part to ε_o and inserting the above expression for η yields:

$$\varepsilon_o = 2\pi N_p R_s d\mu''\omega h_o \left(\frac{R_c - 2\Delta R}{R_c + 2d}\right)$$

where replacing the expression in the parentheses by unity introduces an error of about 5% for our geometry. This signal cannot be compensated out and in fact represents the loss occurring in the copper windings--a problem which has been examined in the text and analyzed in Appendix A.

It is worthwhile pointing out that the signal from the compensator <u>alone</u> which is used to set the lock-in phase to accept only voltage signals in phase with h(t) is shifted from ideality by only $\sim$1.5" of arc at 200 Hz due to the eddy component in the compensator.

It can also be shown that any channel overloading which might occur within the lock-in amplifier due to the coherent signal in quadrature with the one of interest will give rise to at most a small pseudo-hysteretic type term--its W being frequency independent and varying as h_o^2.

Finally, any magnetoresistance that a pick-up coil material might possess can be shown to lead to a weaker than h_o^2 dependence of W_{coil}. The mean resistivity can be written as:

$$\bar{\rho}\ (h_o) \cong \rho_o\ (1 + \alpha h_o^2)$$

where ρ_o is the resistivity in the absence of any applied magnetic field. For $\alpha h_o^2 \ll 1$, $W_{coil} \cong 1.63 \times 10^{-16} \frac{a^3 h_o^2}{\rho_o} (1 - \alpha h_o^2)\nu$ Joule cm^{-2} $cycle^{-1}$ as long as δ (skin depth) >> a.

REFERENCES

1. M. Suenaga and M. Garber, *Science* 18, 952 (1974).

2. A. R. Kaufmann and J. J. Picket, *Bull. Am. Phys. Soc.* 15, 838 (1970).

3. M. Suenaga and W. B. Sampson, *Appl. Phys. Letters* 18, 584 (1971).

4. C. P. Bean, *Rev. Mod. Phys.* 36, 31 (1964).

5. A. M. Campbell, *J. Phys. C: Solid State Phys.* 2, 1492 (1969).

6. S. T. Sekula, *J. Appl. Phys.* 42, 16 (1971).

7. J. C. Male, *Cryogenics* 10, 281 (1970).

8. Y. A. Rocher and J. Septfonds, *Cryogenics* 7, 96 (1967).

9. I. O. Kulik, *Zh. eksp. teor. Fiz. Pis'ma* 3, 398 (1966).

10. N. V. Sarma, *Phys. Lett.* 25A, 318 (1967).

11. U. Krägeloh, *Phys. Stat. Solidi* 42, 559 (1970).

12. P. H. Melville, *J. Phys. C: Solid State Phys.* 4, 2833 (1971).

13. R.M.F. Linford and R. G. Rhodes, *J. Appl. Phys.* 42, 10 (1971).

14. F. Irie, H. Ichikawa and K. Yamafuji, Proceedings of the 3rd Inter. Cryo. Eng. Conf., Iliffe Science and Technology Publications Ltd. Guildford, England (1970), p. 165.

15. D. M. Kroeger, C. C. Koch and J. P. Charlesworth, *J. of Low Temp. Phys.* 19, 493 (1975).

16. J. Sutton, *Proc. Phys. Soc.* 87, 791 (1966).

17. K. Kramer, *Phys. Rev.* 170 (2), 475 (1968).

18. L. D. Landau and E. M. Lifshitz, *Electrodynamics of Continuous Media,* Addison-Wesley, 1960.

FIGURE CAPTIONS

Fig. 1 Sample Induction B Versus Magnetic Field H for Mo-25 at % Re (H_{max} = 756 Oe). T = 4.2K.

Fig. 2 Energy Loss Per Surface Area Per Cycle, W, Versus ac Magnetic Field Amplitude, h_o, for Mo-25 at% Re at 205 Hz. 1650°C Anneal. T = 4.2K. Losses from dc Hysteresis loops are shown for comparison.

Fig. 3 Loss Enhancement Factor, $\frac{W_2-W_1}{W_2}$ Versus Field Amplitude, h_o, for Mo-25 at% Re at 50 Hz.

Fig. 4 Loss Per Surface Area Per Cycle in Copper Pick-Up Coil, W_{Cu}, Versus Square of Magnetic Field Amplitude, h_o^2.

Fig. 5 Induced Voltage Signal in Copper Pick-Up Coil at 500 Hz Versus That at 200 Hz for Common Values of Field Amplitude. Scale is in μv.

Fig. 6 Magnetization Curve of Single Crystal Niobium at T = 4.2K.

Fig. 7 Loss Per Surface Area Per Cycle W_T, Versus Frequency of Applied Magnetic Field, ν. (a) Single Crystal Niobium (b) Low-loss Nb_3Sn. Both sets of data have been corrected for eddy losses in copper pick-up coil.

Fig. 8 Hysteretic Losses Per Surface Area Per Cycle, W_o, in Nb_3Sn Versus Magnetic Field Amplitude, h_o.

Fig. 9 $F(h_o)$ Versus Square of Magnetic Field Amplitude, h_o^2. Data have been corrected for eddy losses in copper pick-up coil. Arrows indicate h_o^*.

Fig. 10 Scanning Electron Micrographs

(a) and (b) Full Field and Edge of high-loss Nb_3Sn

(c) and (d) Full Field and Edge of low-loss Nb_3Sn

(e) and (f) Full Field and Edge of single crystal Nb.

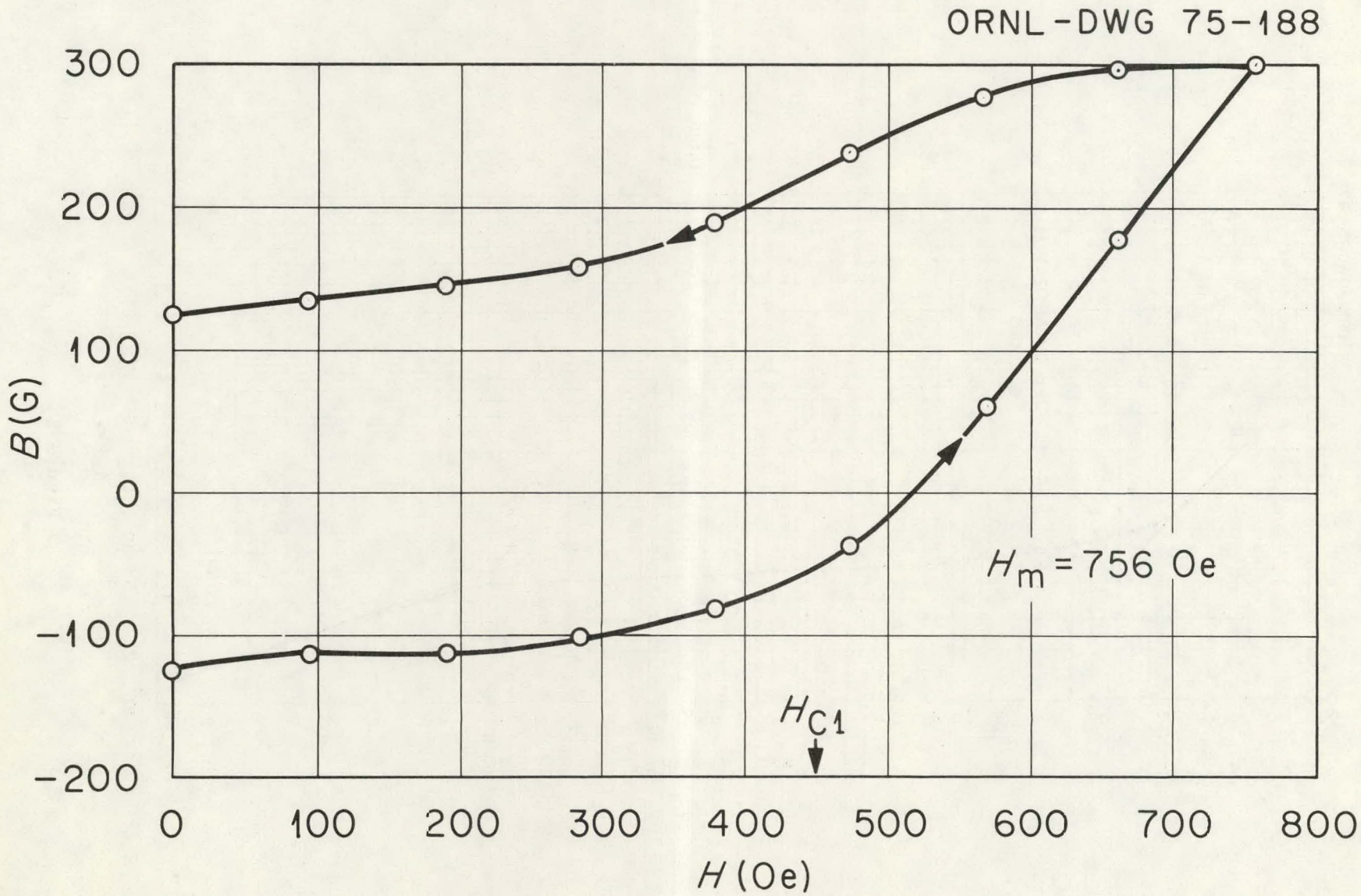
ORNL-DWG 75-188
300
200
100
0
-100
-200
B(G)
0
100
200
300
400
500
600
700
800
H (Oe)
H_m = 756 Oe
H_{C1}

Figure 1

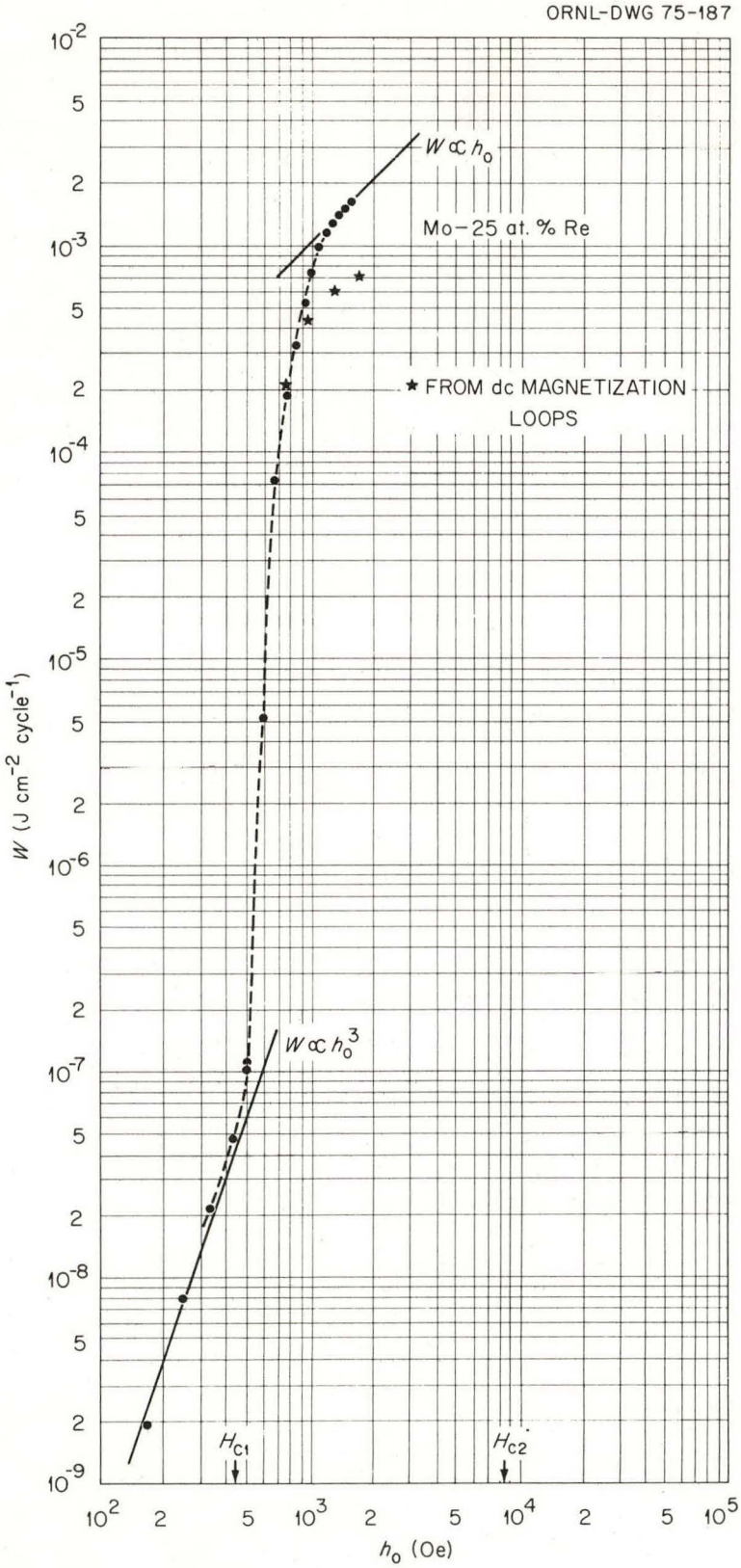
ORNL-DWG 75-187
$W \propto h_0$
Mo–25 at. % Re
★ FROM dc MAGNETIZATION LOOPS
$W \propto h_0^3$
H_{c1}
H_{c2}
W (J cm^{-2} cycle^{-1})
h_0 (Oe)
10^{-2}
10^{-3}
10^{-4}
10^{-5}
10^{-6}
10^{-7}
10^{-8}
10^{-9}
10^2
10^3
10^4
10^5

Figure 2

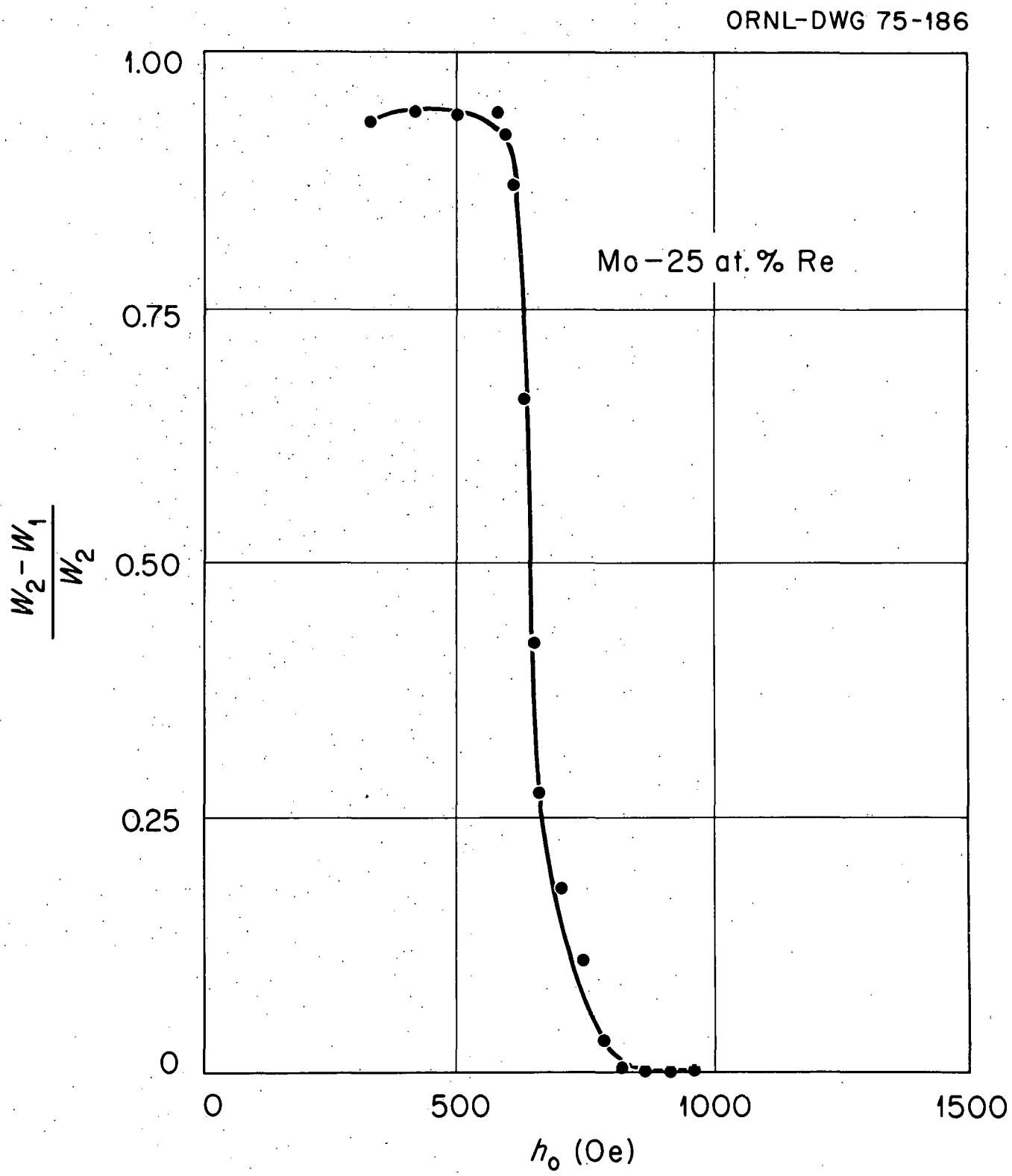
ORNL-DWG 75-186
Mo-25 at.% Re
1.00
0.75
0.50
0.25
0
$\frac{W_2 - W_1}{W_2}$
0
500
1000
1500
h_0 (Oe)

Figure 3

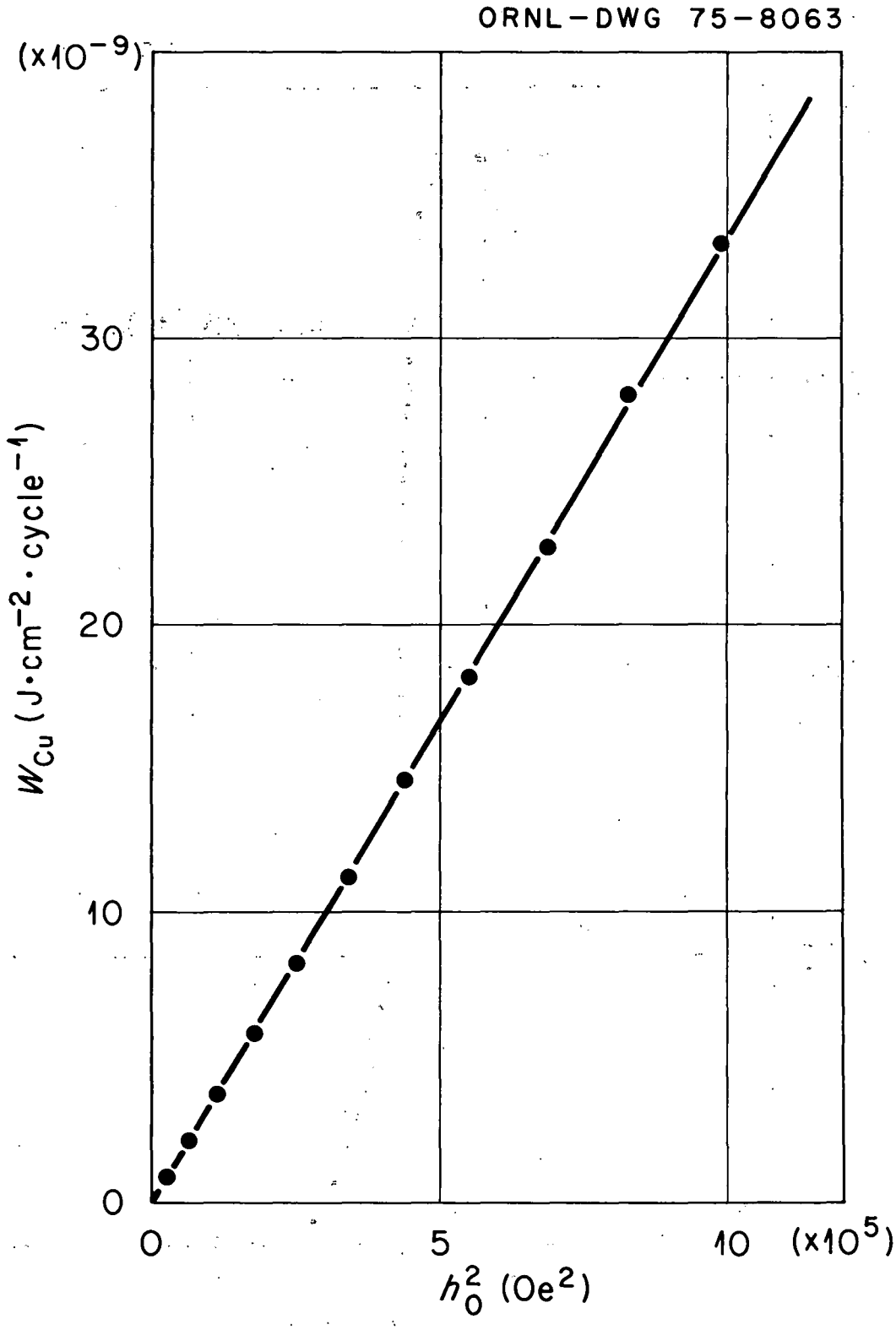
ORNL-DWG 75-8063
(x10^-9)
30
20
10
0
W_Cu (J·cm^-2 · cycle^-1)
0
5
10
(x10^5)
h_0^2 (Oe^2)

Figure 4

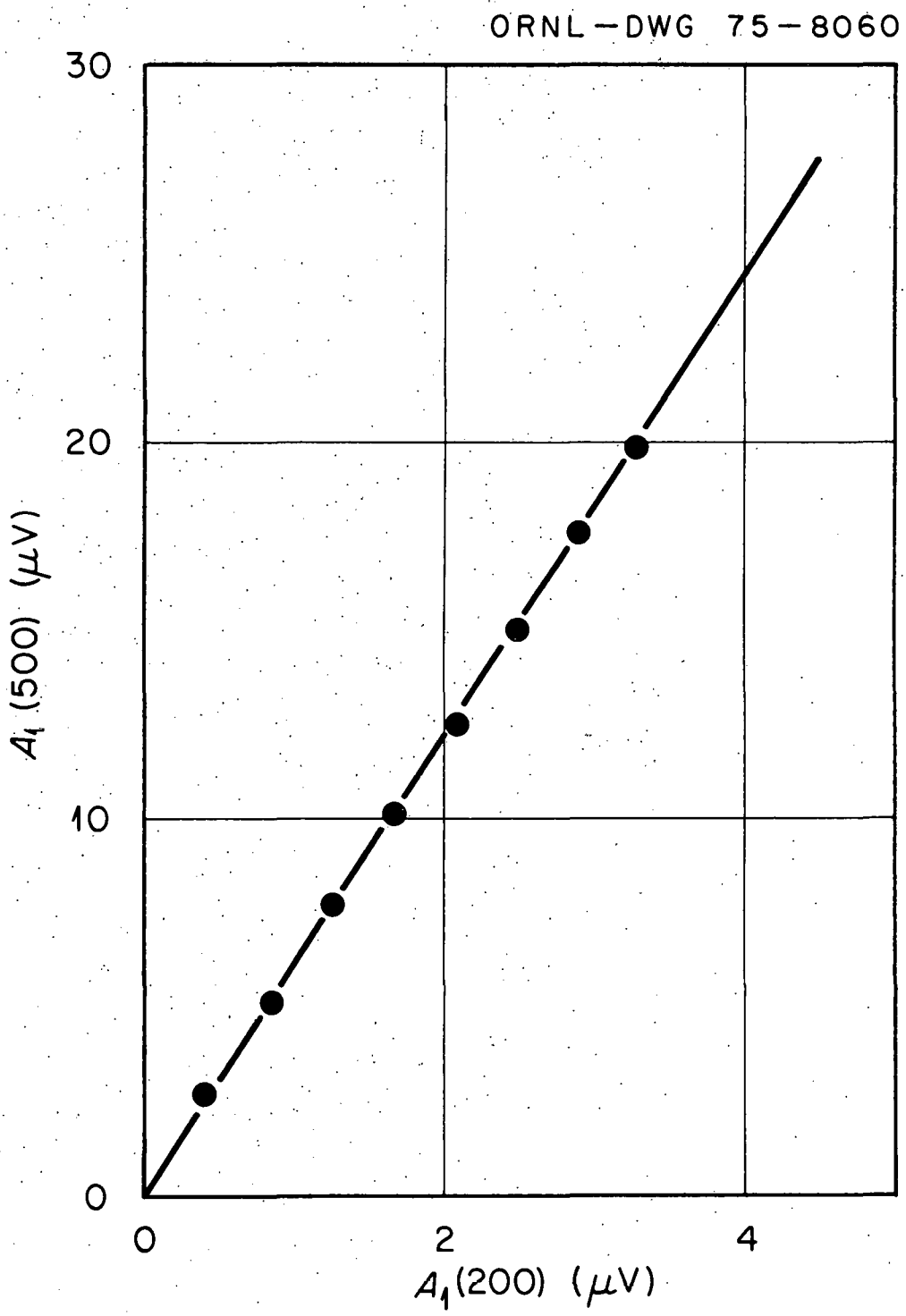

Figure 5

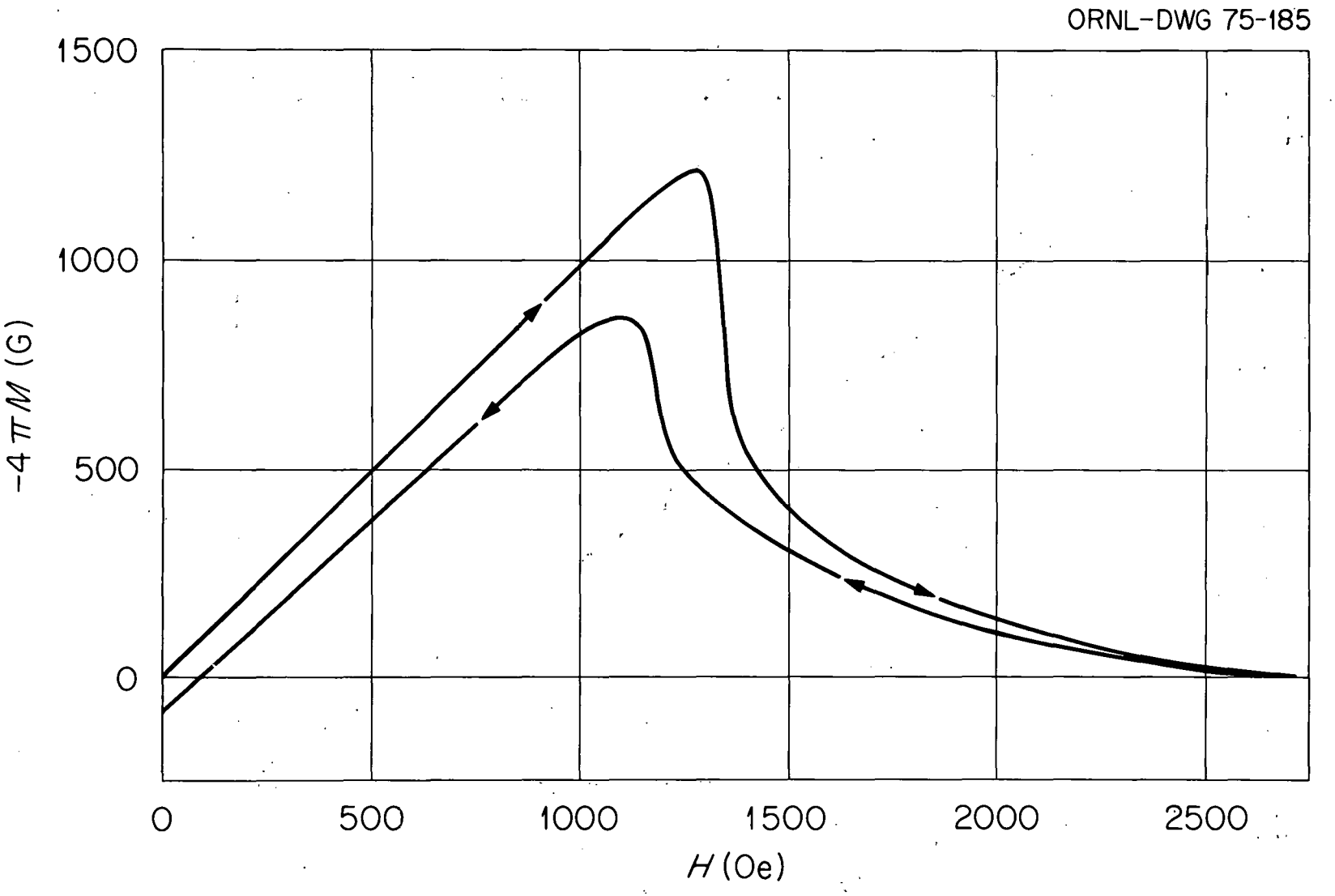
ORNL-DWG 75-185
1500
1000
500
0
$-4\pi M$ (G)
0
500
1000
1500
2000
2500
H (Oe)

Figure 6

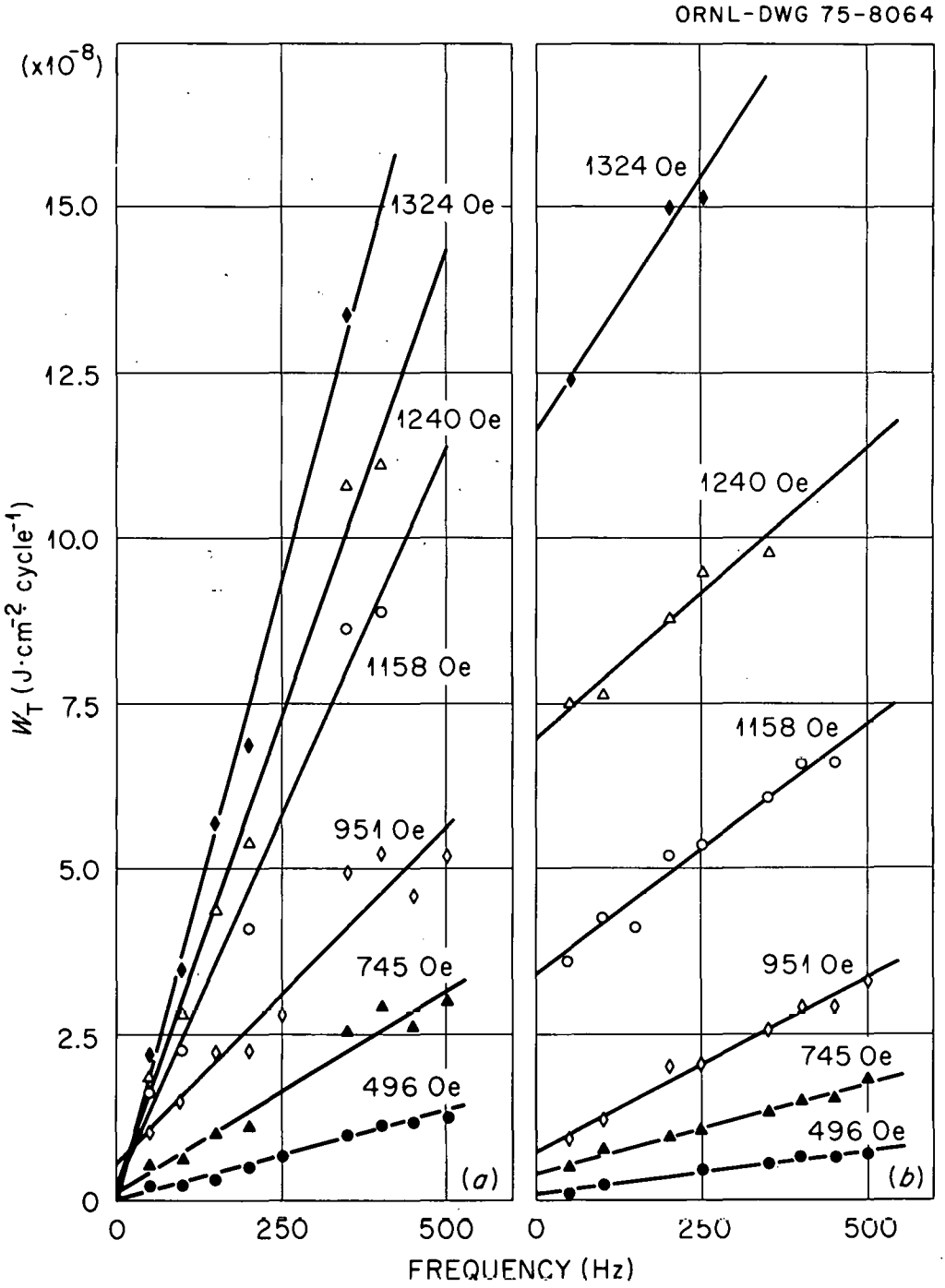
ORNL-DWG 75-8064
(x10^-8)
15.0
12.5
10.0
7.5
5.0
2.5
0
W_T (J·cm^-2 cycle^-1)
1324 Oe
1240 Oe
1158 Oe
951 Oe
745 Oe
496 Oe
(a)
(b)
0
250
500
FREQUENCY (Hz)

Figure 7

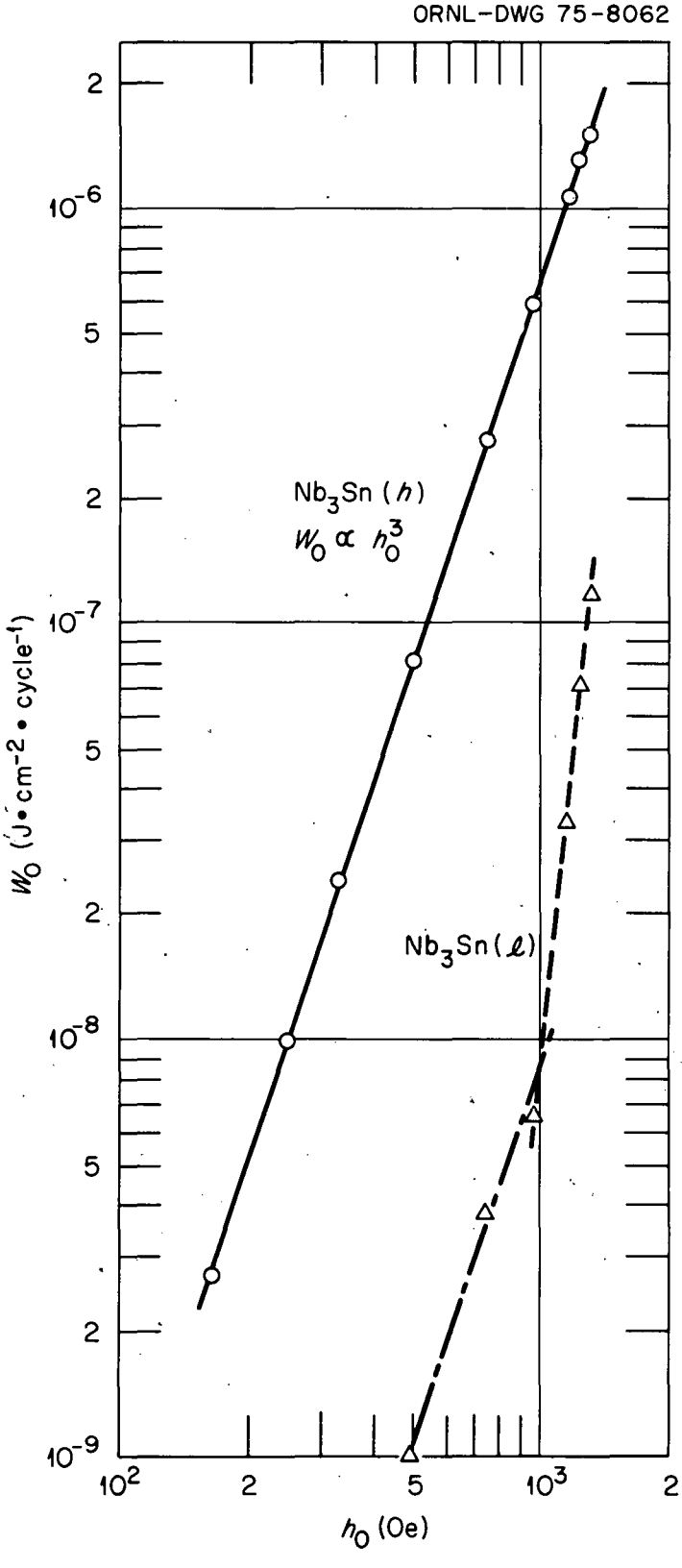
ORNL-DWG 75-8062
Nb_3Sn (h)
$W_0 \propto h_0^3$
Nb_3Sn (ℓ)
W_0 (J • cm^{-2} • cycle^{-1})
h_0 (Oe)
2
10^{-6}
5
2
10^{-7}
5
2
10^{-8}
5
2
10^{-9}
10^2
2
5
10^3
2

Figure 8

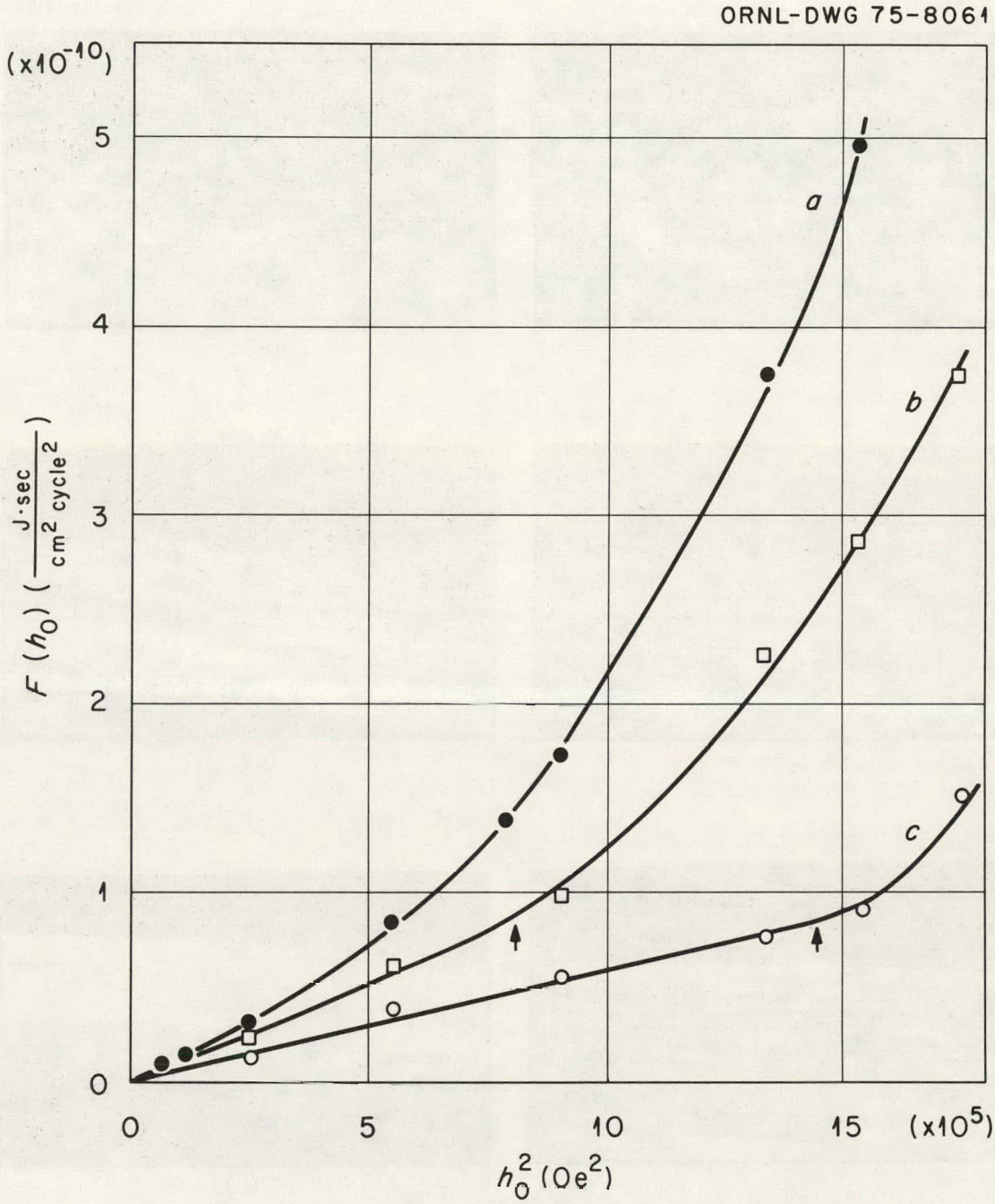
ORNL-DWG 75-8061
(x10^-10)
5
4
3
2
1
0
F (h_0) (J·sec / cm^2 cycle^2)
a
b
c
0
5
10
15
(x10^5)
h_0^2 (Oe^2)

Figure 9

Y-131907

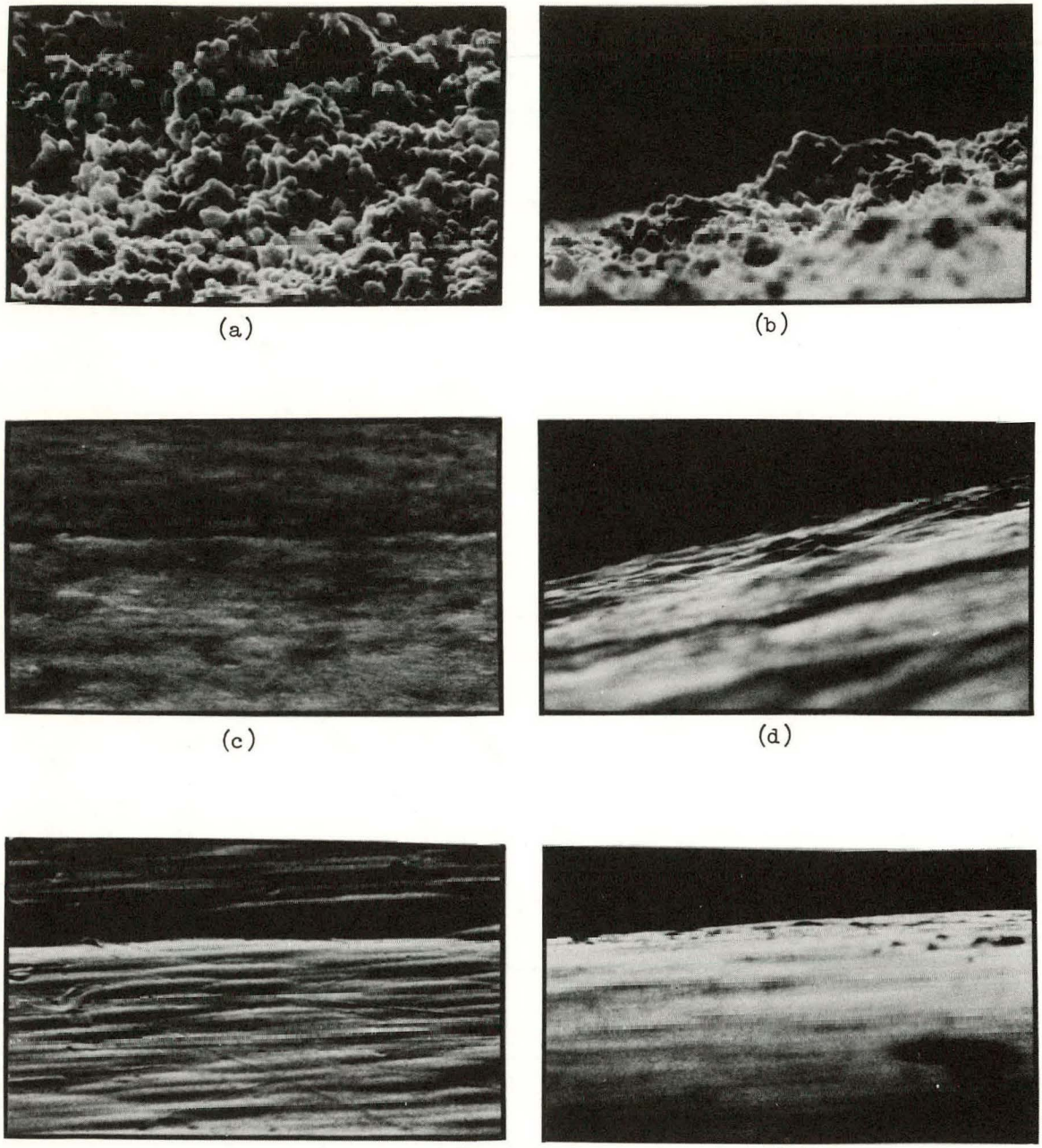

(a) (b) (c) (d) (e) (f)

Figure 10

III. DISPERSION HARDENING OF ALUMINUM

A. Introduction

In the proposed underground superconducting power transmission lines, ultrahigh-purity aluminum is a candidate material for the component serving to carry fault currents and to provide a path for the rated current should the superconductor temporarily go normal. If the aluminum could also mechanically support the superconductor assembly, certain design simplifications and weight savings might be realized. High purity aluminum, though electrically suitable, does not have sufficient strength to accomplish this. It has been the purpose of this research to discover methods for producing a strengthened aluminum while retaining reasonably high conductivity.

We are exploring the possibility of manipulating the dispersant in a dilute, precipitation hardenable alloy whose solid solubility is extremely limited.

B. Residual Resistivity Ratios (RRR)

The initial experiments designed to demonstrate what effect aging has upon the residual resistivity ratio of aluminum-gold alloys were completed during this quarter. A standard four-probe dc technique was used to measure the voltage drop in a wire specimen through which a known current was passed. From this information a resistance could be calculated. Measurements on the same specimen at 273 K (ice-water bath) and at 4.2 K (liquid helium) allowed determination of the residual resistivity ratio, RRR.

Wires of three aluminum-gold alloys containing 0.07, 0.12, and 0.26 wt % gold, respectively, and pure aluminum with no alloying additions were solution heat treated at 600°C for 16 hr in a salt bath and then quenched into an ice-brine solution at near 273 K. Next the quenched specimens were aged in boiling organic liquids or molten salt at temperatures of either 371 K (98°C), 460 K (187°C), or 573 K (300°C) for times of 0.1, 1, 10, 100, or 1000 hr. Figs. 1 through 3 show the variation of RRR with aging time for these alloys at the three aging temperatures. The following characteristics of these data seem noteworthy:

(1) In the solution heat treated and quenched (SHTQ) condition the RRR of the alloys is low due both to the retention of the gold in solid solution and to the production of point defects (vacancies) and defect clusters during the rapid quench. The latter factor is the primary reason the RRR in the pure aluminum is only 3800 rather than 13,000.

(2) Aging at the indicated temperatures causes the RRR to increase in all these materials. Note RRR is plotted on a logarithmic scale. In the alloys this change may be attributable primarily to the precipitation of gold from solid solution.

(3) For the alloys the increase in RRR is greater the higher the aging temperature. The maximum effect was achieved in the 0.12 wt % Au alloy at 573 K (300°C) where RRR increased from 115 to 2674 after aging for 1000 hr. This represents a factor of 23 change in RRR.

4) After SHTQ, pure aluminum can be brought back to its original RRR (∿13,000) by aging for 1 hr at 460 K (187°C) or 0.1 hr at 573 K (300°C) but after 1000 hr at 371 K (98°C) the RRR is back only to 10,000 indicating some quenched-in defects have not yet annealed out.

(5) At aging temperatures of 371 K (98°C) and 460 K (187°C) the 0.12 and 0.07 wt % Au alloys behave very much alike but at 573 K (300°C) that is not the case.

(6) These data suggest that the more substantial changes in RRR occur during aging at the higher temperatures. Additional aging treatments therefore should be carried out at 513 K (240°C) and 623 K (350°C) particularly for the 0.26 and 0.17 wt % alloys.

(7) The fluctuations in the curves plotted in Figs. 1 through 3 need further study. They may merely represent sample-to-sample variations or they may indicate subtle facets of the precipitation process and additional experiments are now underway to verify this. We have also checked the reproducibility of our experimental technique. Repeat runs on the same specimen usually gave RRR's within 1% or less of previous values.

C. Microhardness Measurements

A second set of specimen wires were solution heat-treated, quenched and aged in the manner of the RRR specimens. Vicker's microhardness measurements were made on the cylindrical surface of the wires using a Leitz microhardness tester and loads of either 25, 50, or 100 g. Difficulties were encountered in the softer of the alloys and the pure

aluminum. Reproducibility was poor, hardness values seemed unrealistic and little or no hardness change was detected on aging. Part of the problem may be attributable to the type of wire specimen that was used and the difficulty of measuring hardness in soft materials on cylindrical surfaces. We are currently making up a new set of specimens where microhardness measurements can be made on flat, parallel-sided surfaces. In addition, more measurements will be made on each specimen. This will give us better statistics and improve the precision of the reported values. In spite of these difficulties, microhardness data for the 0.26 wt % Au alloy were considered reasonably good. Fig. 4 depicts how microhardness varied with aging time at 371 K (98°C), 460 K (187°C), and 573 K (300°C) for this alloy. Except for the solution heat treated and quenched condition, these results compare favorably with work by Heimendahl[1] on a 0.2 wt % Au alloy. The important feature is a prominent hardness maximum after 10 hr aging at 187°C. A lesser maximum also occurred at 300°C but at very short times $\leq$ 0.037 hr (4 minutes). The data at 98°C suggest the possibility of two maxima--one at 1 hr, the other at times longer than 1000 hr. More detailed measurements are needed to confirm that possibility, however. The microhardness of the SHTQ specimens was always larger than the results found by Heimendahl.[1] We attribute this difference to specimen size--primarily wire diameter, and quench rate. This point, of course, needs further study.

D. Tensile Testing

Our initial attempts to obtain mechanical property data in the form of stress-strain curves from these alloys indicated an imperative need

to improve our technique. Wires from the RRR studies of pure aluminum and the 0.12 wt % Au alloy in the SHTQ and aged conditions were epoxied to pre-machined brass grips, as shown in Fig. 5. Testing of these tensile specimens caused slippage between the aluminum specimen and the brass grips in spite of being bonded by epoxy. Our inability to use a strain gauge to measure elongation negated the possibility of obtaining the stress-strain curve. Because of the bulkiness of the specimens, it was very difficult not to introduce extraneous or inadvertent deformation into the wires which in all probability would influence the test results. We were able to obtain the ultimate tensile strength (UTS) on four specimens and these are listed in Table I. These values should be considered tentative and their reliability questioned, however. We are now seeking alternate methods of producing tensile specimens and with improved technique we should obtain better data in the future.

E. Composite Materials

Mechanical strengthening of aluminum by means of long fibers embedded within the matrix of the aluminum offers a potentially attractive alternative to the method of strengthening by precipitation hardening in the aluminum-gold alloys. We have received composite samples from two commercial suppliers: AVCO and DWA Composite Specialties, Inc. While the mechanical strengths of these materials are substantial, their electrical properties leave much to be desired. We have measured the RRR of these specimens and Table II summarizes the results. Clearly the commercial composites tested so far do not meet the standards of high RRR required.

TABLE I

Ultimate Tensile Strength (Tentative)

of Aluminum-Gold Alloy at Room Temperature

Material	Condition	UTS (psi)
Pure aluminum	SHTQ + aged 1000 hr at 300°C	4835
Al + 0.12 wt % Au	SHTQ	5872
	SHTQ + aged 10 hr at 300°C	4727
	SHTQ + aged 1000 hr at 300°C	4716

SHTQ = solution heat treated and quenched.

We feel that the quality of the aluminum matrix material and the surface interaction between matrix and fiber need to be given considerable attention before a high RRR composite is possible. To that end, we engaged John Banker of the UCC-ND Y-12 Plant to prepare rods of aluminum composites using our high RRR aluminum as starting material. We have now received specimens prepared by liquid infiltration casting of the following composites:

1. Pure aluminum RRR = 13,000 initially (control)
2. Aluminum with boron fibers
3. Aluminum with boron fibers coated with boron nitride; 3 and 6 vol % fiber.
4. Aluminum with silicon carbide fibers; 3, 6, and 9 vol % fibers.
5. Aluminum with tungsten-3 % rhenium fibers; 2, 3, 6 vol % fibers.

We will be testing these materials for their electrical properties and to determine whether or not atomic diffusion at the fiber/matrix interface caused degradation of the RRR of aluminum.

F. Work in Progress

Further progress depends on whether continued funding will be provided for this program. In addition to the directions already discussed in the previous paragraphs, we would further seek to characterize our materials by means of transmission electron microscopy (TEM). Our intentions are to measure microstructural parameters quantitatively and correlate these with our RRR measurements. We also would emphasize the mechanical testing of our materials.

TABLE II

Results of Specimens

Supplier	Matrix Material	Reinforced Fiber Material	RRR	
			As-Received	Heat Treated 2 hr 525°C
DWA	6061 Al	45 vol % B	3.5	5.4
	OFHC Cu	45 vol % B	93.6	115.3
	202 Al	30 vol % C	2.1	4.4
	Cu-10% Sn	45 vol % C	37.2	92.9
AVCO	Al	B-SiC		
		13.6%	22.2	32.8
		26.6%	17.5	21.5
		43.3%	18.6	23.9

G. Personnel

Personnel associated with the Dispersion Hardening in Aluminum Program during the quarter include the following:

Dr. R. A. Vandermeer, Group Leader, Metals and Ceramics Division

Mr. J. C. Ogle, Technician

REFERENCES

1. M. Heimendahl, *Zeit. für Metallk.* 58, 230 (1967).

FIGURE CAPTIONS

1. Residual resistivity ratios as a function of aging time for an aging temperature of 371 K (98°C).
2. Residual resistivity ratios as a function of aging time at an aging temperature of 460 K (187°C).
3. Residual resistivity ratios as a function of aging time at an aging temperature of 573 K (300°C).
4. Microhardness as a function of aging time for Al + 0.26 wt % Au alloy aged at 371 K (98°C), 460 K (187°C), and 573 K (300°C).
5. Close-up of tensile specimen.

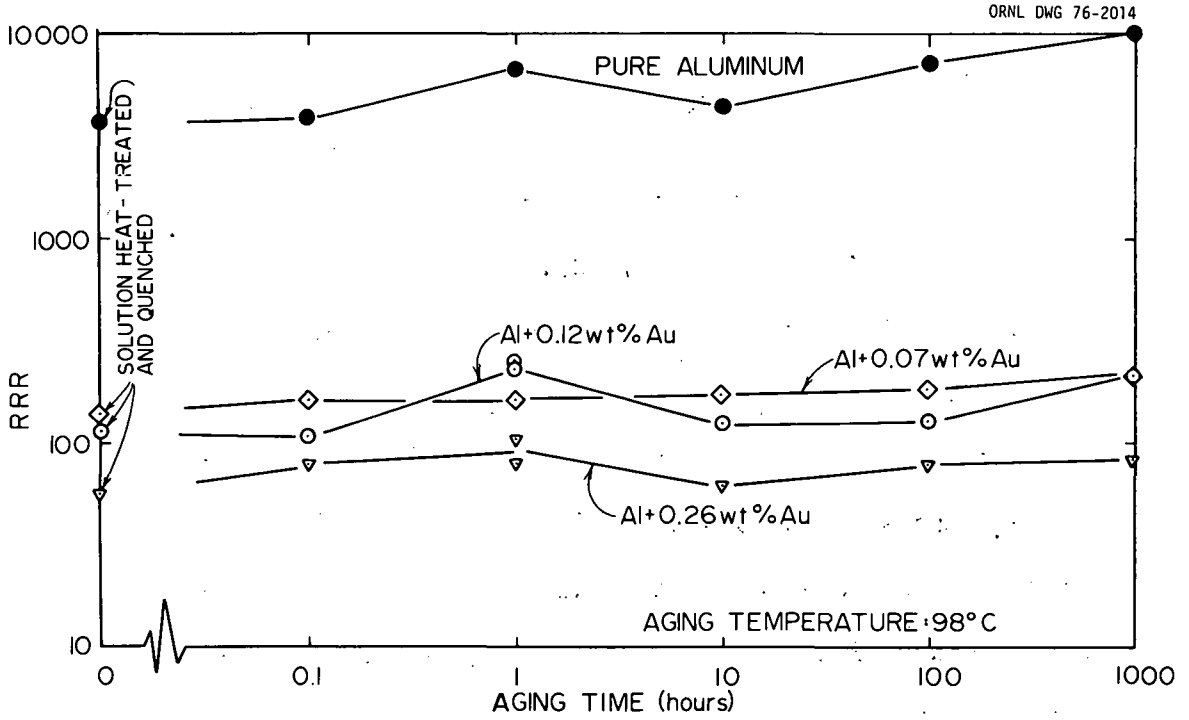

Figure 1

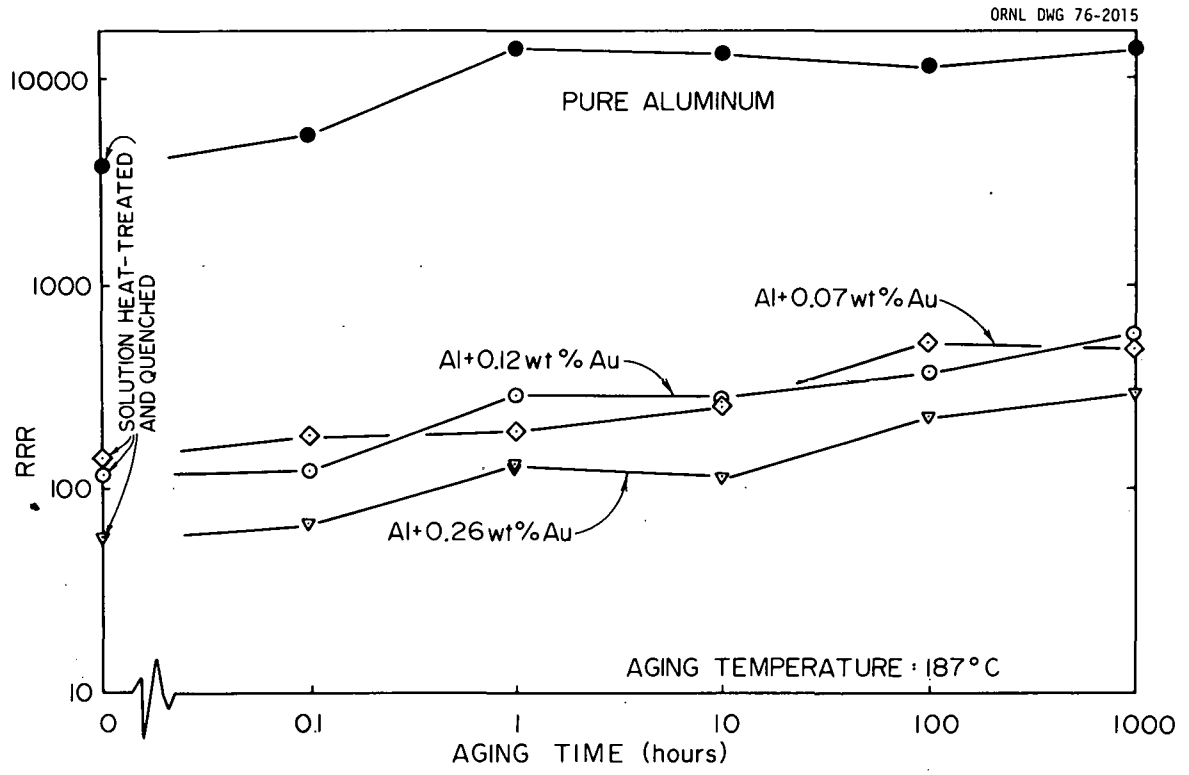

Figure 2

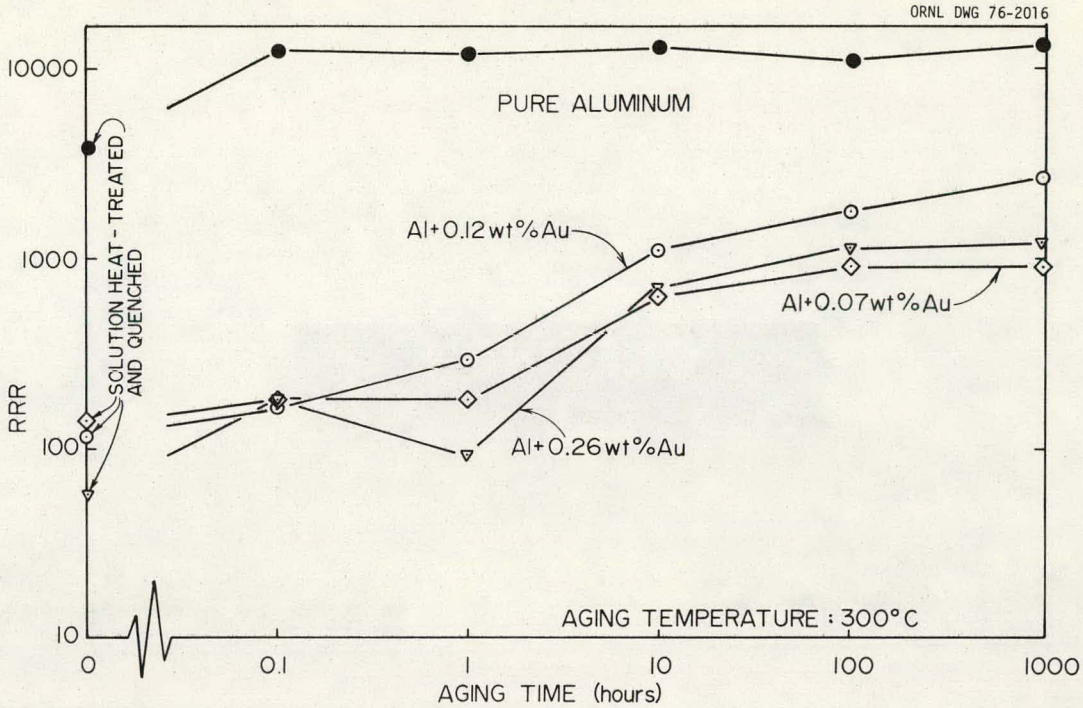

Figure 3

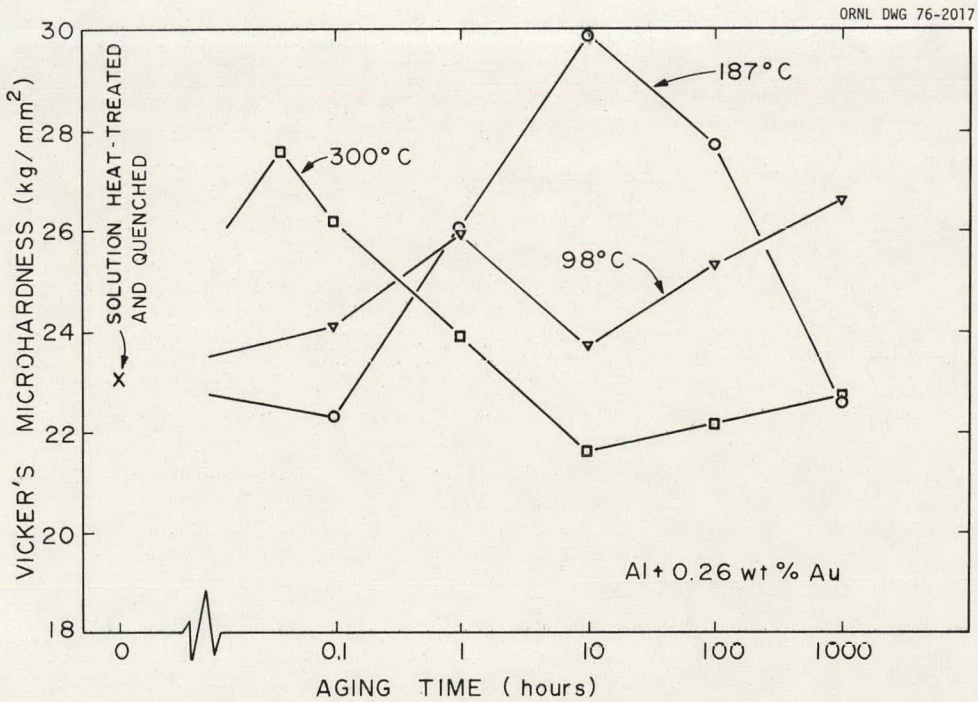

Figure 4

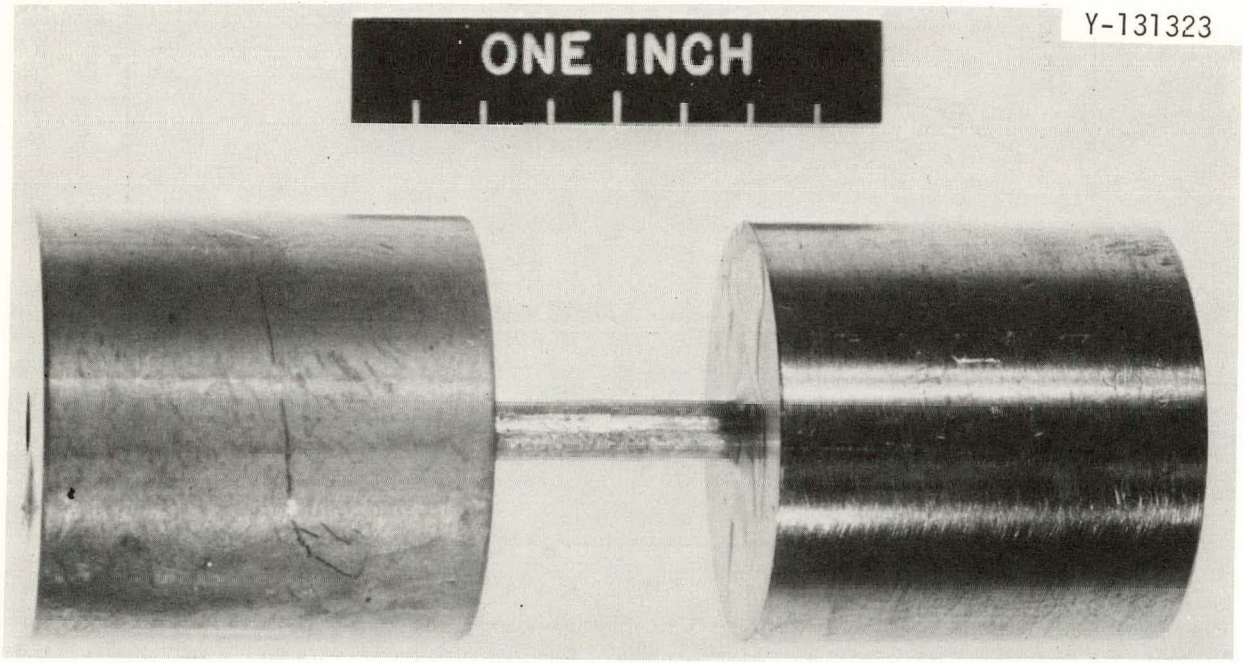

Figure 5

Internal Distribution

1. S. E. Beall
2. J. Blevins (ERDA-ORO)
3. L. G. Christophorou
4. Document Reference Section, Y-12
5. G. G. Kelley
6. R. H. Kernohan
7. C. C. Koch
8.-10. Laboratory Records
11. Laboratory Records RC
12. J. A. Lenhard (ERDA-ORO)
13.-14. CR Library
15. R. S. Livingston
16.-37. H. M. Long
38. M. M. Menon
39. F. L. Miller
40. O. B. Morgan
41. ORNL Patent Office
42. S. W. Schwenterly
43. S. T. Sekula
44. Thermonuclear Division Library
45. R. A. Vandermeer
46. A. Zucker

External Distribution

47. G. Bogner, Siemens AG Research Laboratories, 852 Erlangen, Germany
48. J. M. Bonneville, Hydro-Quebec Institute of Research Technical Engineering and Thermodynamics Laboratory, P.O. Box 1000, Varennes, Quebec, Canada Jol 2 PO
49. R. Boom, University of Wisconsin, 513 Engineering Research Building, 1500 Johnson Drive, Madison, WI 53706
50.-53. Dr. Alvin Clorfeine, Division of Electric Energy Systems, U.S. Energy Research and Development Administration, 20 Massachusetts Avenue N.W., Mail Station G-234, Washington, D.C. 20545
54. C. M. Cooke, Massachusetts Institute of Technology, High Voltage Research Laboratory, Building N-10, Cambridge MA 02139
55. E. D. Eich, Power Technologies, Inc., Box 284, Milwood, NY 10546
56.-82. ERDA TIC, P.O. Box 62, Oak Ridge, TN 37830
83.-86. E. B. Forsyth, Brookhaven National Laboratory, Upton, L.I., NY 11973
87. E. O. Forster, Esso Research and Engineering Co., P.O. Box 45, Linden, NJ 07036
88. M. Fukasawa, Hitachi Cable, Ltd. Research Laboratory, The 1st Department 5-1, Hitaka-cho, Hitachi-shi, Ibaraki-ken, Japan

89. E. Garwin, Stanford Linear Accelerator Center, Stanford University, P.O. Box 4349, Stanford, CA 94305
90. W. F. Gauster, Neuwaldeggerstrasse 11-11-5 A, 1170 Vienna, Austria
91. P. Graneau, Underground Power Corp., 205 Holdenwood Road, Concord, MA 01742
92. David Hartmann, Bonneville Power Authority, P.O. Box 3621, Portland, OR 97208
93. R. L. Hirsch, ERDA, Division of Controlled Thermonuclear Research, Washington, D.C. 20545
94. C. H. Hoogerhyde, Public Service Gas & Electric Co. of New Jersey, 80 Park Place, Newark, NJ 07101
95. M. Jeffries, General Electric Co., P.O. Box 43, Bldg. 37, Room 365, Schenectady, NY 12301
96. M. Jones, National Bureau of Standards, Institute for Basic Standards, Cryogenic Division, 275.00, Boulder, CO 80302
97. W. F. Keller, Los Alamos Scientific Laboratory, University of California, P.O. Box 1663, Los Alamos, NM 86544
98. C. N. King, Stanford University, Department of Applied Physics, Stanford, CA 94305
99. P. Komarek, Kernforschungszentrum Karlsruhe, Institut fur Experimentelle Kernphysik III, D75 Karlsruhe, Postfach 3640, Germany
100. S. Linke, Cornell University, School of Electrical Engineering, 204 Phillips Hall, Ithaca, NY 14850
101. B. Maddox, Central Electricity Research Laboratories, Electrical Engineering Division, Kelvin Avenue, Leatherhead, Surrey, England
102. R. Meyerhoff, Union Carbide Corp., Technical Center, Linde Research Laboratories, Tarrytown, NY 10591
103. J. Nichol, Arthur D. Little Company, Inc. 20 Acorn Park, Cambridge, MA 02140
104. Oskars Petersons, National Bureau of Standards, High Voltage Measurement Section, Bldg. 22C, Room B-344, Washington, D.C. 20234
105. Dr. T. Praehauser, Roemer Str. 4, 4147 Aesch. Bl, Switzerland
106. Mario Rabinowitz, Electric Power Research Institute, 3412 Hillview Avenue, Palo Alto, CA 94304
107. E. H. Reynolds, British Insulated Callenders Cables, Ltd., 38 Wood Lane, London W12 7DX, England
108. C. H. Rosner, Intermagnetics General Corp., Charles Industrial Park, New Karner Road, Guilderland, NY 12084
109. Dr. George M. L. Sommerman, 2402 Collins Road, Pittsburgh, PA 15235
110. Z. J. J. Stekly, Magnetic Corporation of America, 179 Bear Hill Road, Waltham, MA 02154
111. D. K. Stevens, DPR-ERDA, Washington, D.C. 20545
112. C. E. Taylor, L-382, Lawrence Livermore Laboratory, P.O. Box 808, Livermore, CA 94550

113. Dr. B. M. Weedy, Electrical Engineering Dept., The University Southampton, United Kingdom
114. Dr. W. F. Westendorp, 17 Front Street, Schenectady, NY 12305
115. Dr. R. Wimmershoff, AEG-Telefunken Kabelwerke Ag, Muelheim, W. Germany
116. J. Wong, Supercon, Inc., 9 Erie Drive, Natick, MA 01760
117. A. Zanona, Commonwealth Edison Company, Technical Center, 1319 South First Avenue, Maywood, IL 60153

☆ U.S. GOVERNMENT PRINTING OFFICE: 1976-748-189/232